Tunnelling and Underground Space Technology 154 (2024) 106111

Contents lists available at ScienceDirect

Tunnelling and Underground Space Technology incorporating Trenchless Technology Research

journal homepage: www.elsevier.com/locate/tust

Effect of internal pressure on the flexural fatigue behaviour of trenchless internal replacement pipe systems

Shanika Kiriella [a], Allan Manalo [a], Cam Minh Tri Tien [a], Hamid Ahmadi [a,*], Warna Karunasena [a], Patrick G. Dixon [b], Ahmad Salah [a], Brad P. Wham [b]

[a] Centre for Future Materials, University of Southern Queensland, Toowoomba, QLD 4350, Australia
[b] Center for Infrastructure, Energy, and Space Testing, University of Colorado, Boulder, CO 80309, USA

ARTICLE INFO

Keywords:
Trenchless technology
Gas pipelines
Internal replacement pipe (IRP)
Repetitive load transmitted from vehicular traffic
Internal pressure
Flexural fatigue
Finite element analysis (FEA)

ABSTRACT

Internal replacement pipe (IRP) systems are a novel trenchless technique that is gaining interest in the rehabilitation of damaged legacy pipelines distributing natural gas. Performance evaluation of IRP systems under repetitive loads transmitted from vehicular traffic is essential to ensure their optimal and safe design. This study conducted numerical simulations to examine the impact of internal pressure on the bending fatigue behaviour of IRP systems that are fully bonded to legacy gas pipes with circumferential discontinuities. Other design parameters include the thickness and modulus of elasticity of IRP and the level of transmitted traffic load. The findings indicate that the operating internal pressure has a greater impact on the longitudinal stresses than the circumferential stresses of IRP when subjected to cyclic bending. The level of internal pressure changes the failure behaviour of IRP under fatigue. Based on the results obtained from extensive parametric simulations, mathematical expressions were formulated to predict the fatigue life of the IRP systems. Contour plots were generated to represent fatigue life response for different combinations of internal pressure levels and transmitted traffic loads.

1. Introduction

Pipelines have been extensively utilised for transporting gas and oil over long distances, primarily due to their high transportation capacity, cost efficiency and safety (Deng et al., 2022; El-Abbasy et al., 2015; Shamsuddoha et al., 2013; Alabtah et al., 2021; Rohem et al., 2016). Underground pipelines are susceptible to damage and failure during their service life because of various factors, including but not limited to ageing, corrosion, construction defects, third-party disruption and operational errors (Velázquez et al., 2022; Kraidi et al., 2019; Xu et al., 2023; Chen et al., 2019; Chin and Lee, 2005; Abd-Elhady et al., 2020; Zhang and Wong, 2023). Circumferential crack is the most prevalent failure in pipes with a smaller diameter (< 380 mm or 14.96 in) (Makar et al., 2001). This type of crack is primarily caused by stresses induced by ground deformation during trench construction (Makar et al., 2001; Jeon et al., 2004). Metal loss due to corrosion can also cause circumferential cracks in legacy pipes (Akhi and Dhar, 2021; Shirazi et al., 2023). Internal replacement pipe (IRP) systems are a novel and developing trenchless rehabilitation technology that has been introduced for repairing bare steel and cast-iron legacy gas pipelines with circumferential cracks, discontinuities, or pulled-out joints (Dixon et al., 2023; Fu et al., 2022). This repair technique involves the insertion of a new structural pipe into existing pipes that contain defects and discontinuities. The integration of IRP systems yields significant enhancements in the structural integrity and restores the service life of legacy pipelines. This type of repair system is cost-effective, environmentally friendly, and requires less construction time (Allouche et al., 2014; Lu et al., 2020; Li et al., 2023; Fuselli et al., 2022; Yahong et al., 2023). However, the design and the development of IRPs should ensure their ability to endure various forms of loading, throughout their service life.

Based on the existing literature, the most common failure mechanisms related to IRPs in host pipe systems are as follows: fatigue failure caused by repetitive traffic loading (Guo et al., 2005; Tafsirojjaman et al., 2022; Wang et al., 2019), lateral deformation due to surface loads

* Corresponding author.
E-mail addresses: shanika.kiriella@unisq.edu.au (S. Kiriella), allan.manalo@unisq.edu.au (A. Manalo), camminhtri.tien@unisq.edu.au (C.M.T. Tien), hamid.ahmadi@unisq.edu.au (H. Ahmadi), karu.karunasena@unisq.edu.au (W. Karunasena), padi9036@colorado.edu (P.G. Dixon), ahmad.salah@unisq.edu.au (A. Salah), brad.wham@colorado.edu (B.P. Wham).

https://doi.org/10.1016/j.tust.2024.106111
Received 4 June 2024; Received in revised form 1 September 2024; Accepted 27 September 2024
Available online 3 October 2024

(Jeon et al., 2004; Tafsirojjaman et al., 2022; Argyrou et al., 2019; Vasseghi et al., 2021; Vazouras et al., 2012; Liu et al., 2019; Melissianos et al., 2017; Alzabeebee et al., 2018), localised fracture and leakage due to internal pressure (Tafsirojjaman et al., 2022; Mattos, H.d.C., J.M.L. Reis, L.M. Paim, M.L.d. Silva, R.L. Junior, and V.A. Perrut, 2016; Budhe et al., 2020) and axial deformation resulting from thermal stresses (Tafsirojjaman et al., 2022; Bokaian, 2004; Zhong et al., 2018). Among these failure modes, fatigue failure caused by high cyclic/repetitive surface loads from vehicular traffic is considered one of the most severe conditions for the host pipes and IRP system (Dixon et al., 2023; Tafsirojjaman et al., 2022). The wheel loads, which are directly above the pipes and move parallel to their longitudinal axis, are transmitted to underground pipes through the soil (Jeon et al., 2004; Stewart et al., 2015). When such loads are applied, the IRP system may be susceptible to maximum deformation and stress at the weakest discontinuity in the host pipeline. Prolonged exposure to cyclic stresses can reduce the strength of an IRP system and can compromise its structural integrity. This process can lead to fatigue failure, where the IRP may fracture even under stress levels lower than its ultimate strength. Thus, having an in-depth understanding of fatigue behaviour and accurate life estimation of IRP systems is a crucial aspect in the design and development of new and emerging IRP systems.

Currently, there is a lack of comparable standards or guidelines related to internal composite pipe repair systems (Tafsirojjaman et al., 2022). In addition, only a few studies have been conducted on the bending fatigue behaviour of legacy pipes that have undergone repair utilizing liners, especially in cases where the host pipes have circumferential crack discontinuities or pulled-out joints (Jeon et al., 2004; Stewart et al., 2015; Ha et al., 2016). New and emerging IRP systems are currently under development, utilising a range of materials such as polymeric coating, thermoplastic, and fibre-reinforced polymer (FRP) composite (Tafsirojjaman et al., 2022). However, there are only a limited number of studies available on these systems. The existing studies primarily focus on either cured-in-place pipe (CIPP) liners (Jeon et al., 2004; Stewart et al., 2015) or spray-applied pipe liners (SAPL) (Ha et al., 2016) with low elastic modulus and low thickness in comparison to the host pipe. By conducting experimental three-point cyclic bending tests, Jeon et al. (2004) examined the fatigue performance of 0.25 mm (0.01 in) thick CIPP lined 152.4 mm (6.0 in) diameter cast iron (CI) pipe with a low internal pressure of nitrogen gas under one million loading cycles with a maximum vertical displacement of 2.5 mm (0.1 in). The liner was fully bonded to the host pipe, and there was 75 % stiffness degradation after one million cycles, but no failures were observed. Stewart et al. (2015) performed four-point cyclic bending tests of 2.5 mm (0.1 in) thick CIPP liners that were fully bonded to 152.4 mm (6.0 in) and 304.8 mm (12.0 in) diameter CI pipes with joints under one million loading cycles with maximum deflections of 1.52 mm (0.06 in) and 1.78 mm (0.07 in), respectively while maintaining an operating pressure of 102 kPa (14.8 psi). These systems were subjected to a predetermined number of cycles in accordance with service life requirements, rather than being cycled until failure, during which a decrease in stiffness was observed. The flexural fatigue behaviour of a 150.0 mm (5.91 in) diameter steel host pipe with a 25.0 mm (0.98 in) wide circumferential crack that was repaired with 3.0 mm (0.12 in) thick SAPL under a cyclic vertical displacement of 0.3 mm (0.01 in) with an internal water pressure of 12.0 kPa (1.7 psi) was studied by Ha et al. (2016). Despite the observation of stiffness degradation in the system throughout the testing, Ha et al. (2016) found no failure or leakage in the lined pipe.

Available studies on the fatigue behaviour of repaired pipes were conducted under low internal pressure levels. According to Tien et al. (2023), the maximum operating internal pressure of the legacy steel pipe can be 413.7 kPa (60.0 psi), and their maximum allowable internal pressure can be 1379.0 kPa (200.0 psi). In their study, Tien et al. (2023) investigated the effect of crack edges on a steel host pipe with a diameter of 323.85 mm (12.75 in) on the behaviour of a thermoplastic IRP under an internal pressure of 1379.0 kPa (200.0 psi). The IRP had a thickness of 3.175 mm (0.125 in) and a modulus of elasticity (MOE) of 5.0 GPa (725 ksi). The width of the crack opening was measured to be 914.4 mm (36.0 in). It was found that under internal pressure alone, the IRP underwent bending as it curved around the crack edge of the host pipe, resulting in a concentration of longitudinal stresses. Unlike the crack edge region, the opening region of IRP is primarily influenced by hoop stress. The results of these studies suggest that the fatigue life of IRP may be negatively affected by the application of internal pressure during cyclic bending, particularly, in cases where the host pipe has circumferential cracks or discontinuities.

Brown et al. (2014) used finite element analysis (FEA) to examine the performance of a 5.0 mm (0.2 in) thick CIPP liner placed in a circumferentially cracked CI host pipe under an internal pressure of 689.5 kPa (100 psi). The analysis revealed a significant concentration of axial stresses in the liner along the edge of the host pipe, where its structural integrity had been compromised. Shou and Chen (2018) and Shou and Huang (2020) investigated the effect of internal pressure on the static bending behaviour of steel pipes with circular corrosion defects repaired by CIPP liners with a MOE of 13.0 GPa (1885 ksi) under a vehicular load of 350.0 kN (78.7 kips). The defects found in the host pipes had a maximum diameter of 100.0 mm (3.94 in) and were located either on the upper or lateral surface. Shou and Chen (2018) and Shou and Huang (2020) discovered that maximum von Mises stress at the defect increases nonlinearly when the internal pressure is increased from zero to 588.4 kPa (85.3 psi). It was also shown that under static bending, the internal pressure causes a localized accumulation of longitudinal stresses at the damaged area.

The fatigue behaviour of an IRP could potentially be influenced by their wall thickness, MOE and the magnitude of the traffic load. In a recent study conducted by Tafsirojjaman et al. (2022) the behaviour of IRP alone made of various materials with MOE ranging from 1.0 GPa (145.0 ksi) to 200.0 GPa (29,007.5 ksi) and wall thicknesses ranging from 3.175 mm (0.125 in) to 25.4 mm (1.0 in) under repetitive traffic load of 17.4 kN (3.9 kips) was numerically investigated. They found that an increase in both MOE and wall thickness can significantly improve the fatigue life of IRP. Based on the outcomes of an experimental cyclic bending testing on carbon fibre-reinforced polymer (CFRP) pipe with thicknesses of 5.0 mm (0.2 in) and 11.2 mm (0.44 in), Huang et al. (2020) demonstrated that the CFRP pipes do not exhibit failure even after one million cycles when subjected to a load of 43.6 kN (9.8 kips) whereas those exposed to a relatively higher load (87.0 kN or 19.6 kips) failed before reaching the anticipated design life of one million cycles. However, these existing studies have focused on the behaviour of non-pressurized IRP alone even though the operating internal pressure may have a detrimental effect on the behaviour of the repair pipe during cyclic bending, particularly in the existence of the damaged host pipe. According to the parametric studies on the effect of internal pressure alone and combined effect of surface load and internal pressure, Shou and Chen (2018) found that reducing the thickness of CIPP liner from 10.0 mm (0.39 in) to 5.0 mm (0.2 in) greatly increased the stress at the circular corrosion defect, while Shou and Huang (2020) discovered that, increasing MOE of the liner from 13.0 GPa (1885.5 ksi) to 130.0 GPa (18,854.9 ksi) and thickness from 3.8 mm (0.15 in) to 6.2 mm (0.24 in) led to a reduction in stress concentration at the circular corrosion defect. The effects of these parameters on IRP used for rehabilitating host pipes with circumferential discontinuities need to be investigated under fatigue loading.

The studies from the literature indicated that the flexural fatigue phenomenon creates a bottleneck in the design and development of new and emerging IRP systems system due to a lack of literature and design standards. Consequently, the behaviour of IRP systems installed in host pipes with circumferential cracks or discontinuities under cyclic loads transmitted from vehicular traffic, along with the selection of the most appropriate material and geometric properties must be thoroughly examined. The objective of this study is to numerically investigate how

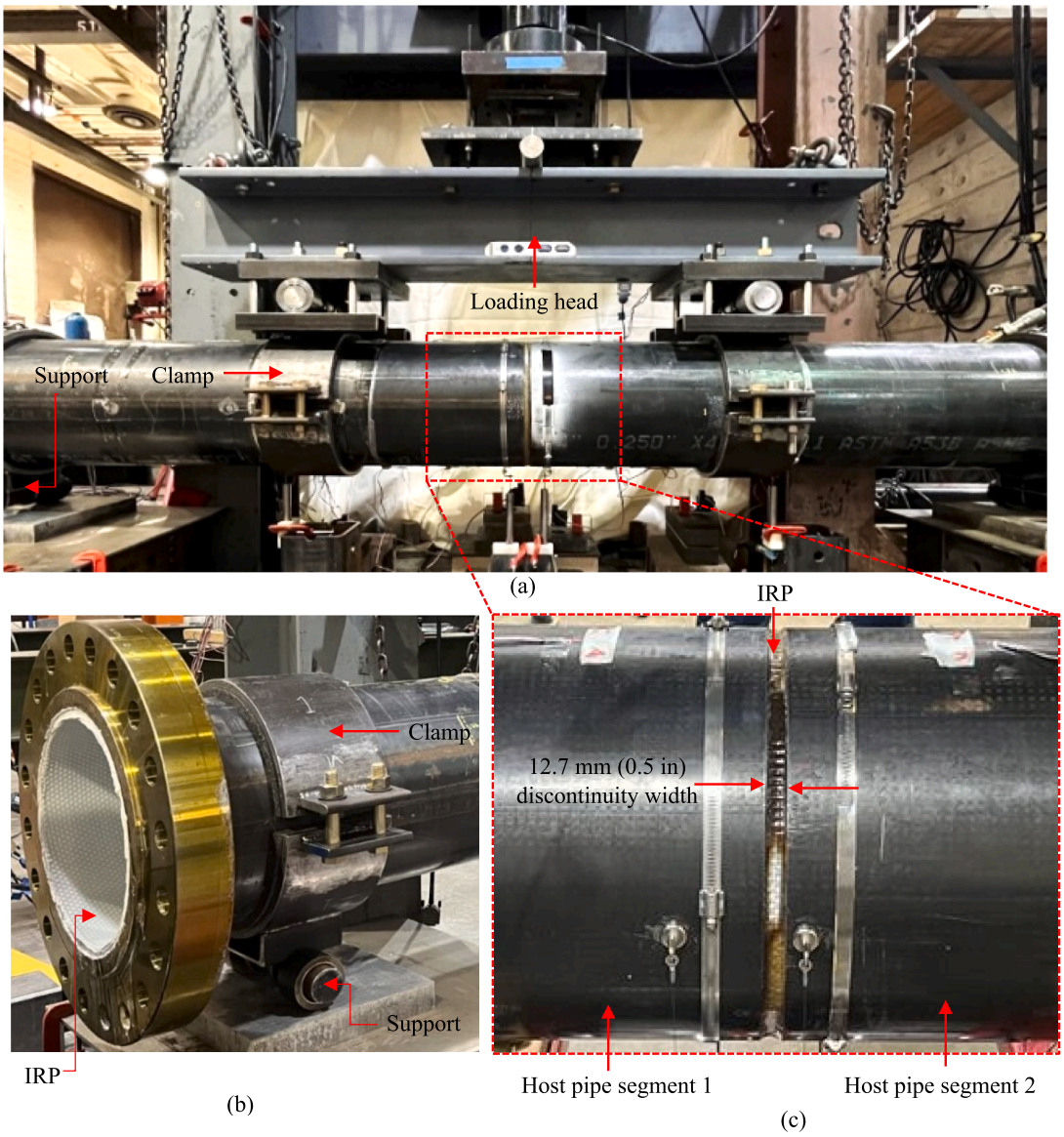

Fig. 1. (a) Actual four-point bending test setup developed by CUB, (b) pipe end and support, (c) circumferential host pipe discontinuity at the midspan.

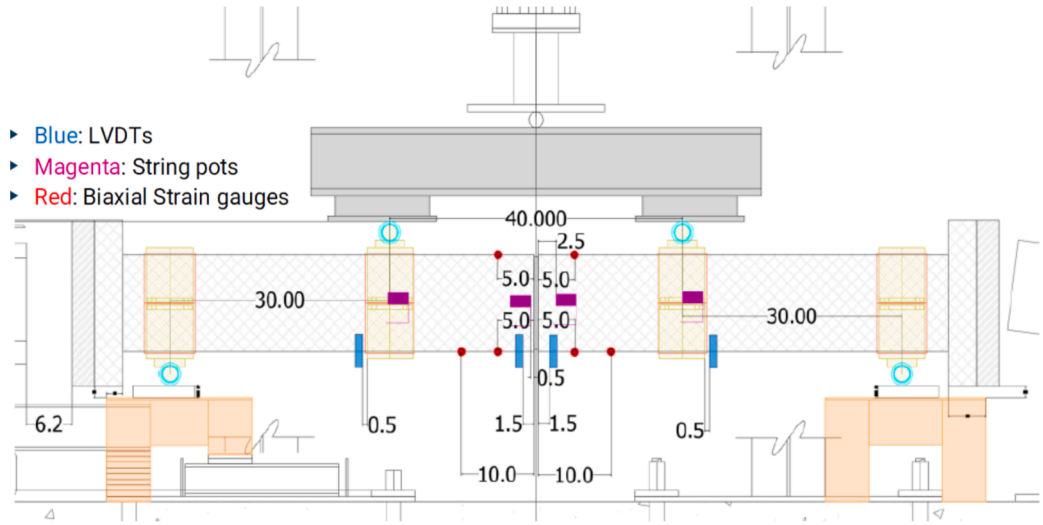

Fig. 2. Schematic diagram of the bending test setup with the locations of strain gauges and linear variable differential transformers (LVDTs) (CUB) [Units: in].

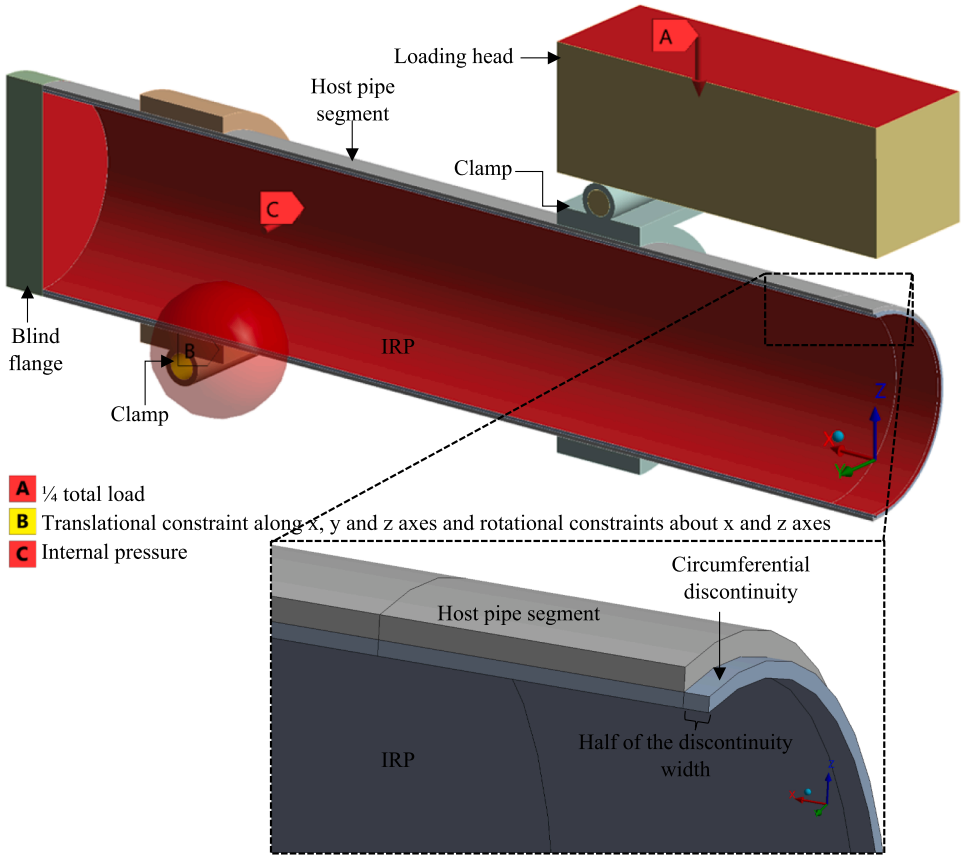

Fig. 3. Quarter symmetry FE model of an IRP installed within a host pipe that has a circumferential discontinuity at its midspan.

internal pressure influences the bending fatigue behaviours of IRPs that are fully bonded to the host pipes with circumferential discontinuities at the midspan under repetitive loads transmitted from vehicular traffic. The investigations were carried out by varying design parameters such as the thickness and MOE of the IRP and the level of the transmitted traffic load. By utilising the results obtained from extensive parametric investigations, mathematical equations that can predict the fatigue life of the IRP systems were established. Contour plots were generated by employing the derived equations to graphically represent the fatigue life response under different combinations of internal pressure and transmitted traffic loads. The outcomes of this study will assist pipeline developers and designers in delivering safe, reliable and cost-effective trenchless IRP repair systems, which are in high demand within the pipeline industry.

2. Methodology

2.1. Finite element modelling and analysis

Finite element (FE) models of four-point bending test in three dimensions (3D) are executed using ANSYS Mechanical (Ansys, 2021) to replicate the experimental configuration of IRP-repaired host pipe systems with discontinuities under transmitted traffic loading over 50 years of service life. The simulations employ parameters that are identical to those used in the four-point bending test setup developed by the University of Colorado Boulder (CUB), as shown in Figs. 1 and 2. The host pipe in the FE model has a full circumferential discontinuity at the midspan. The present study employs a 12.7 mm (0.5 in) wide narrow discontinuity that was identified as critical under static bending of IRP

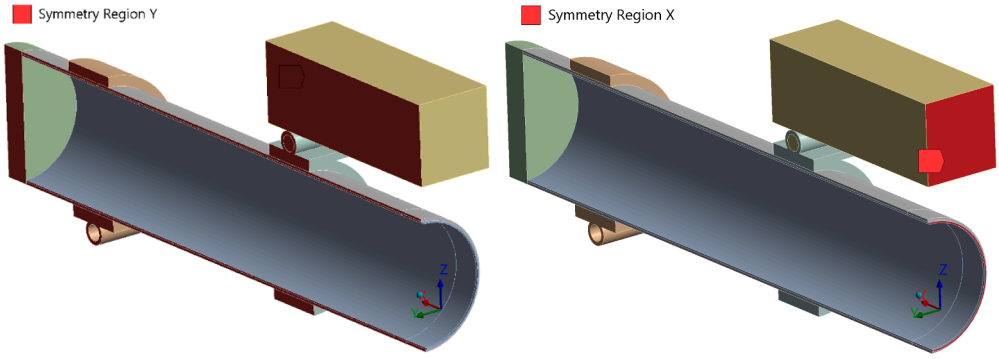

(a) Constrained translational degree of freedom perpendicular to the XZ symmetry plane

(b) Constrained translational degree of freedom perpendicular to the YZ symmetry plane

Fig. 4. Symmetry planes and constraints.

Table 1
Properties of IRP and host pipe materials.

Component	Material	MOE		Poisons ratio	Reference
		GPa	ksi		
IRP	Polymer	1.7	246.6	0.11	Mellott and Fatemi (2014)
	GFRP-1	3.7	536.6	0.23	Laboratory testing
	GFRP-2	7.9	1145.8	0.25	Zakaria et al. (2016)
	GFRP-3	14.0	2030.5	0.25	Huh et al. (2012)
	GFRP-4	26.4	3829.0	0.25	Huh et al. (2012)
	GFRP-5	38.6	5598.5	0.25	Huh et al. (2012)
Host pipe	Steel	200	29007.5	0.29	Preedawiphat et al. (2020)

systems in an investigation conducted by Kiriella et al. (2023). This discontinuity width indicates the presence of a pulled-out but operational joint in legacy pipelines. The host pipe has an outer diameter of 323.85 mm (12.75 in) and a wall thickness of 6.35 mm (0.25 in), both of which are kept at constant values throughout the study. While the outer diameter of the IRP, which is determined by the inner diameter of the host pipe, is held constant at 311.15 mm (12.25 in), the wall thickness is varied during the investigation.

Due to the symmetry of the geometry, material orientation, loading, boundary conditions, and expected responses about both XZ and YZ planes, only one-quarter of the actual bending setup is modelled (Fig. 3). This reduces the analysis run time and memory requirement while increasing the accuracy of the results by using a finer mesh. The translational degree of freedom perpendicular to the XZ and YZ symmetry planes (mirror planes) of the quarter symmetry model is constrained using the symmetry region feature in ANSYS Mechanical (Fig. 4). A pinned support containing a frictionless connection between the host pipe and clamp is implemented to ensure a precise representation of experimental test configuration while mitigating potential convergence problems. Additionally, the loading head is attached to another clamp through the employment of a pin-lug mechanism. The models implemented in this study do not incorporate the surrounding soil, which is regarded as the most critical condition. However, the impact of soil above the system is integrated into the models by applying the level of load transmitted through soil from vehicular traffic (14.8 kN (3.3 kips)) as determined by Klingaman et al. (2022). In their evaluation of transmitted traffic load, Klingaman et al. (2022) followed the procedure recommended by Petersen et al. (2010) for assessing the live load distribution on buried concrete culverts. This level of loading, when repeated one million cycles, is representative of the transmitted traffic load that an IRP system is anticipated to experience during a 50-year service life. It should be noted that, due to the implementation of a quarter symmetry model, only a load that is equal to one-fourth of the total load is exerted on the loading head.

Standard SOLID186, a higher-order 3D solid element with 20 nodes, is used in the modelling of IRP systems. Steel is utilised for the host pipe, whereas several IRP materials, including unreinforced polymer, and glass fibre-reinforced polymer (GFRP) composites are employed (Table 1). Steel is also used for all other components such as clamps, lugs, pins and loading head. The analyses are conducted employing linear elastic isotropic material behaviour, under the assumption that the IRP material properties are consistent in both longitudinal and hoop direction directions. Additionally, it is assumed that both polymeric and FRP composites have a failure strain limit of 0.02 (Tafsirojjaman et al., 2022; Sirimanna et al., 2015).

The current investigations employ the stress-life approach, considering that the anticipated design life of IRP is one million loading cycles (Jeon et al., 2004; Stewart et al., 2015). The stress life approach involves analysing the model under static loading conditions to determine the stresses generated in the IRP. Subsequently, the fatigue tool available in

Table 2
Data sources for the S-N curves and stress ratios of IRP materials.

Material	Stress ratio	Reference
Polymer	−1	Mellott and Fatemi (2014)
GFRP-1	0.1	Laboratory testing
GFRP-2	0.1	Zakaria et al. (2016)
GFRP-3	0.1	Huh et al. (2012)
GFRP-4	0.1	Huh et al. (2012)
GFRP-5	0.1	Huh et al. (2012)

ANSYS Mechanical is employed to simulate the fatigue induced by repetitive loading. This tool computes the effective alternating stresses by taking into account the maximum and minimum stresses obtained from the static analysis. The extent of the damage caused by a loading cycle is determined based on both the alternating stresses and mean stress (Fajri et al., 2021; Nieslony and Bohm, 2013). In the current study, Goodman's mean stress correction theory (Fajri et al., 2021; Puigoriol-Forcada et al., 2018; Ferdous et al., 2020; Zhang et al., 2018; Susmel et al., 2005) is applied to account for the effect of mean stress on the stress amplitude. The corrected alternating stress also referred to as effective alternating stress, is subsequently mapped onto the Stress-life (S-N) curves of the IRP material to identify the alternating stress at the point of failure and determine the corresponding number of cycles. If the number of cycles is below 1 million, it is considered that the IRP will fail before the design life is reached. The fatigue life analysis, considering the combined influence of traffic load and internal pressure, relies on S-N curves derived from uniaxial fatigue testing conducted in both longitudinal and transverse orientations. This approach was chosen due to the high cost and complexity associated with conducting multiaxial fatigue tests. S-N curves for polymeric, GFRP-2, GFRP-3, GFRP-4 and GFRP-5 repair materials were gathered from the literature (Table 2), while the stress-life behaviour of GFRP-1 material in both the longitudinal and transverse directions (as shown in Fig. 5(a) and (b), respectively) was generated by conducting fatigue tests according to ASTM D3479/D 3479 M (ASTM, 2019). The stress ratio of the polymeric IRP is −1, while that of all GFRP materials is 0.1 (Table 2). In this investigation, the applied loading has a constant amplitude and a zero-based loading ratio.

The analysis conducted focuses on IRP systems that are fully bonded to the discontinuous host pipes. To establish a completely bonded connection between the two components in the FE model, the IRP and host pipe segments are connected together along their entire interface using the "bonded" connection type in ANSYS Mechanical. The bonded connection type ensures that there is no sliding or separation between the faces or edges of the components. The normal and tangential forces exert significant resistance against external forces that could potentially cause relative motion between surfaces. During the process of cyclic bending, it is possible for debonding to occur at the discontinuity, leading to a reduction in stress concentration at the discontinuity edges. In the present study, however, it is assumed that throughout the entire service life, the bond between the host pipe and IRP remains intact, with no debonding or detachment occurring at the interface. This assumption is made to ensure that the current study focuses on analysing the most critical condition that can be caused by high-stress concentrations as was observed in previous studies (Kiriella et al., 2023; Kiriella et al., 2024).

Fig. 6 shows the mesh that was generated for the FE model with quarter symmetry. A 10.0 mm (0.39 in) element size is employed for the loading head, clamps and blind flange. A refined mesh with an element size of 1.6 × 1.6 mm (0.06 × 0.06 in) is applied to IRP within the discontinuity and to both IRP and host pipe across a length of 76.2 mm (3.0 in) beyond the edge of the discontinuity to accurately capture the potential stress concentrations. Outside these refined regions, an element size of 5.0 × 5.0 mm (0.2 × 0.2 in) is used. The mesh size along the wall thickness of the two pipes is set at three elements. These element sizes for the mesh of each component are selected based on a

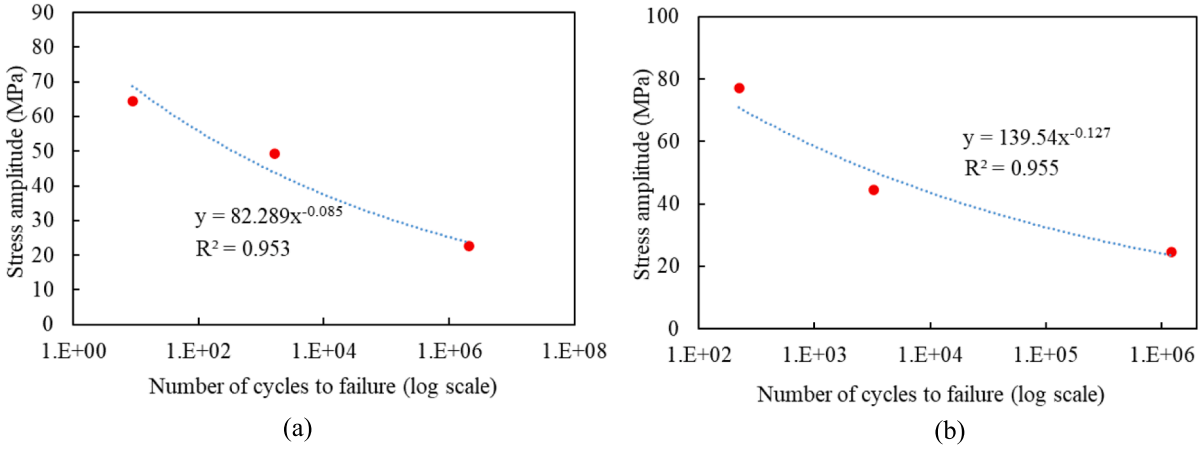

Fig. 5. S-N curve of GFRP-1 obtained from dog bone specimens that were cut in a manner where their lengths aligned with (a) longitudinal direction of IRP (MOE of 3.739 GPa or 542 ksi) and (b) circumferential direction of IRP (MOE of 9.7 GPa or 1407 ksi).

mesh convergence and sensitivity analysis conducted by Kiriella et al. (2024).

In the analysis, the internal pressure is varied from 0 to 620.5 kPa (90.0 psi) in increments of 206.8 kPa (30.0 psi). The selected internal pressure levels cover the maximum operating internal pressure of 413.7 kPa (60.0 psi), as reported by Tien et al. (2023), as well as pressure levels that are both below and above this threshold by 206.8 kPa (30.0 psi) in addition to the non-pressurised condition. The IRP thicknesses considered are 3.175 mm (0.125 in), 4.115 mm (0.162 in), 6.35 mm (0.25 in) and 9.525 mm (0.375 in), while the MOE values are 1.744 GPa (253 ksi) (polymer), 3.739 GPa (542 ksi) (GFRP-1), 7.9 (1146 ksi) (GFRP-2), 14.03 GPa (2035 ksi) (GFRP-3), 26.4 GPa (3833 ksi) (GFRP-4) and 38.63 GPa (5603 ksi) (GFRP-5). The different levels of transmitted traffic loading are 10.0 kN (2.2 kips), 14.8 kN (3.3 kips), 20.0 kN (4.5 kips) and 25.0 kN (5.6 kips). These parameters are based on Kiriella et al. (2024).

2.2. *Effectiveness of using hot-spot stress and localized stress for determining fatigue life*

The effectiveness of employing hot-spot stress (HSS) and the localized stress at the discontinuity edge of IRP-repaired host pipe systems for fatigue life estimation is examined under the combined influence of bending and internal pressure in accordance with the study conducted by (Kiriella et al. (2024)). To accomplish this, IRP installed in discontinuous host pipe systems are subjected to a transmitted traffic load of 14.8 kN (3.3 kips) while their internal pressure remains constant at zero, 206.8 kPa (30.0 psi), 413.7 kPa (60.0 psi) and 620.5 kPa (90.0 psi). As shown in Fig. 7, a comparison is made between the resulting HSS and localised stress in IRP at the discontinuity edge on the tension side. The figure shows that when the internal pressure is increased, both HSS and localized stress at the discontinuity edge exhibit a comparable trend. The maximum discrepancy between the HSS and the localized stress is approximately 8%, which is deemed negligible for this type of scenario. While the HSS approach is widely acknowledged as suitable for determining the maximum stress at a discontinuity of a segment, its application for the extensive parametric investigation of fatigue life in the current study is found to be more challenging and time-consuming. This is because each scenario requires the manual computation of the highest alternating stress and the corresponding fatigue life. However, if localised stress is considered, the minimum fatigue life of the system can be directly obtained from the ANSYS fatigue tool. Consequently, even if the localised stress may be slightly over-conservative, falling within an 8% range of the HSS value, it can still be considered a reasonable estimate. Therefore, instead of HSS, local stress is used for fatigue life analysis in this study due to its ability to achieve a balance of practicality and accuracy while effectively meeting the requirements of the analysis.

2.3. *Validating the numerical model*

The accuracy of the FE results is ensured through validation with laboratory experimental results from the University of Colorado Boulder. The present study consists of a comparison between the load–strain (Fig. 8) and load–deflection (Fig. 9) behaviours of a GFRP-1 IRP installed in a steel host pipe with a discontinuity width of 12.7 mm (0.5 in) under a cyclic bending load of 14.3 kN (3.2 kips) obtained from FEA and laboratory experiments. The results are extracted from multiple locations at the crown and invert of both the left and right halves of the IRP. The distances to each location in both Fig. 8 and Fig. 9 are measured from the midspan. The load–strain and load–deflection behaviours obtained from FEA are in good agreement with experimental results, as depicted in Fig. 8 and Fig. 9, respectively.

3. Results and discussion

3.1. *Longitudinal stresses, hoop stresses and fatigue lives*

The IRP repair system undergoes a combination of bending stress caused by bending moment and hoop stress resulting from the internal pressure when it is under internal pressure and exposed to cyclic bending. The longitudinal and hoop stress at the discontinuity edge and the midspan of the IRP, as the internal pressure increases, are demonstrated in Fig. 10. GFRP-1 is utilized to conduct this analysis with a repair thickness of 4.115 mm (0.162 in) while the internal pressure is varied between zero and 620.5 kPa (90.0 psi) under a transmitted traffic loading of 14.8 kN (3.3 kips). The figure shows that longitudinal and hoop stresses at the discontinuity edge and the midspan at the bottom of IRP (invert) are in tension and increase almost linearly, while those at the top (crown) are in compression and decrease linearly. The reason for such behaviour is that when internal pressure is present, it creates forces along the pipe length, which elongate IRP in the axial direction, inducing longitudinal stresses. In the tensile region (bottom), this additional longitudinal stress induced by internal pressure couples to the bending stress, producing a relatively higher tensile stress than in the system without internal pressure. In the compression region (top) of IRP, the bending stresses reduce the longitudinal stresses induced by internal pressure resulting in relatively lower compressive stress than in the system without internal pressure. Since the magnitude of the longitudinal stress induced is proportional to the internal pressure applied, an increasing internal pressure under the same level of transmitted traffic load leads to a rise in longitudinal stresses, which ultimately results in an

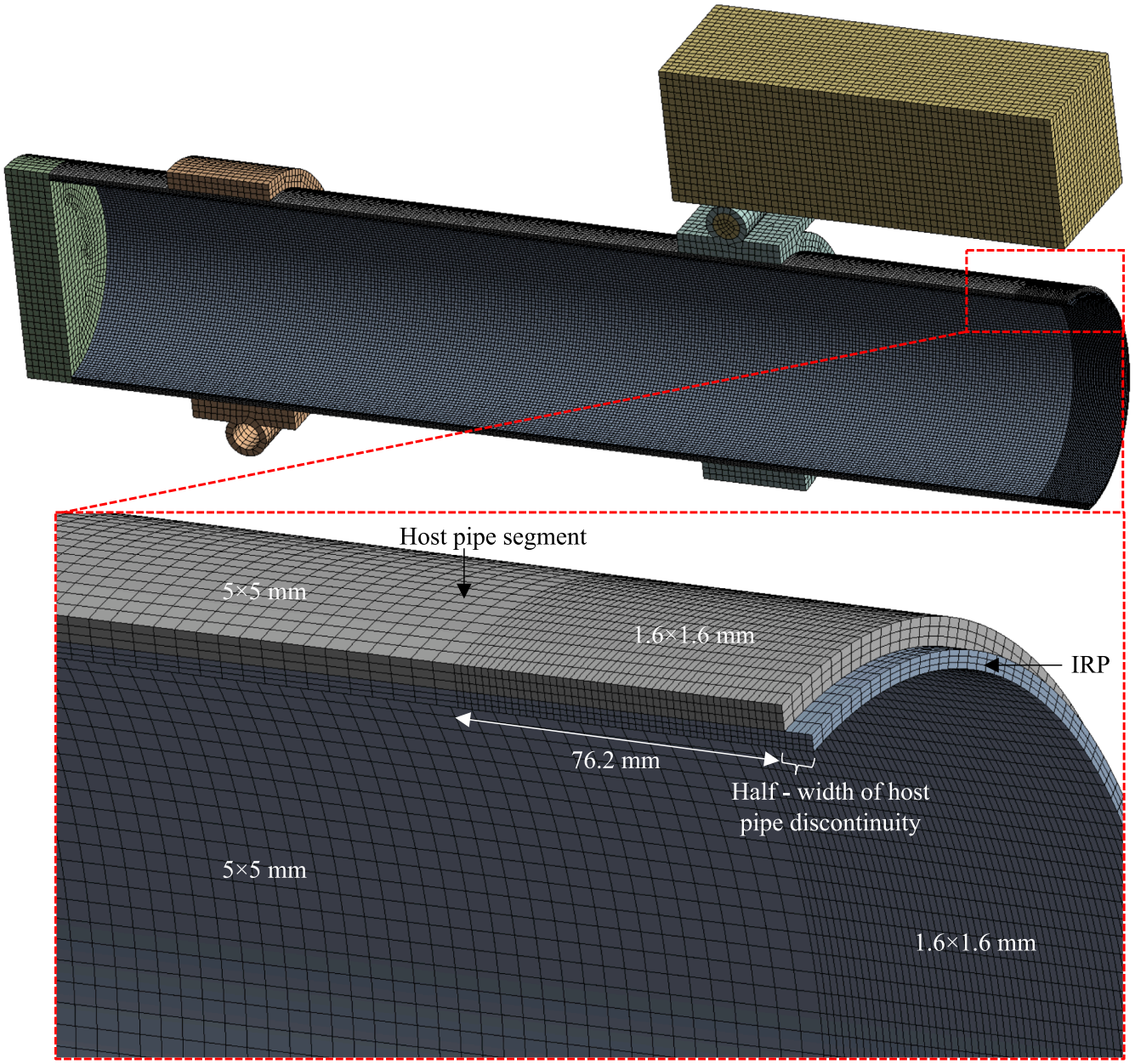

Fig. 6. Mesh refinement of quarter symmetry FE model of an IRP inserted in host pipe with 12.7 mm (0.5 in) wide discontinuity.

overall increase in tensile stresses while a decrease in compressive stresses in IRP.

Under all internal pressure levels, longitudinal stresses are higher than the corresponding hoop stresses at each of the locations on IRP being considered. At all the internal pressure levels, longitudinal tensile stress at the bottom of IRP at the discontinuity edge is the dominant stress during bending fatigue when the system is fully bonded, which is similar to that without internal pressure (Fig. 11). Without internal pressure, the lower portion of IRP at midspan exhibits a slight bulging effect between the discontinuity edges of the host pipe, while the upper portion undergoes a minor inward bending as depicted in Fig. 11. As the internal pressure increases, the bulge at the bottom of IRP becomes more pronounced due to the increase in longitudinal tensile stress while the inward bending at top diminishes because of the decrease in longitudinal compressive stress (Fig. 12). The overall increase in the critical stress at the discontinuity edge at the bottom as the internal pressure rises from zero to 620.5 kPa (90.0 psi) is around 72%. According to Tien et al. (2023), it is possible to reduce the stress concentration due to internal pressure at the discontinuity edge by not bonding the IRP to the host pipe up to a certain length. This approach allows the unbonded length of the IRP to slide relatively within the host pipe, enabling more effective formation around the discontinuity edge compared to the fully bonded scenario. Additionally, rounding the edges of the host pipe can reduce potential stress concentration in bonded IRP systems.

Table 3 presents a comparison of fatigue life between the circumferential and longitudinal stresses for a 4.115 mm (0.162 in) thick GFRP-1 IRP subjected to a transmitted traffic load of 14.8 kN (3.3 kips) under different levels of internal pressure. The fatigue life of IRP, based on maximum alternating stress in the longitudinal direction and corresponding S-N behaviour at an internal pressure of zero, 206.8 kPa (30.0 psi), 413.7 kPa (60.0 psi) and 620.5 kPa (90.0 psi) are determined to be 2.7E+06, 1.2E+05, 8492 and 869 cycles, respectively. In contrast, even when exposed to an internal pressure of 620.5 kPa (90.0 psi), the fatigue life of IRP, determined based on the maximum alternating stress in the circumferential direction and corresponding S-N behaviour, exceeds one billion cycles. This is because the circumferential stresses that arise in an

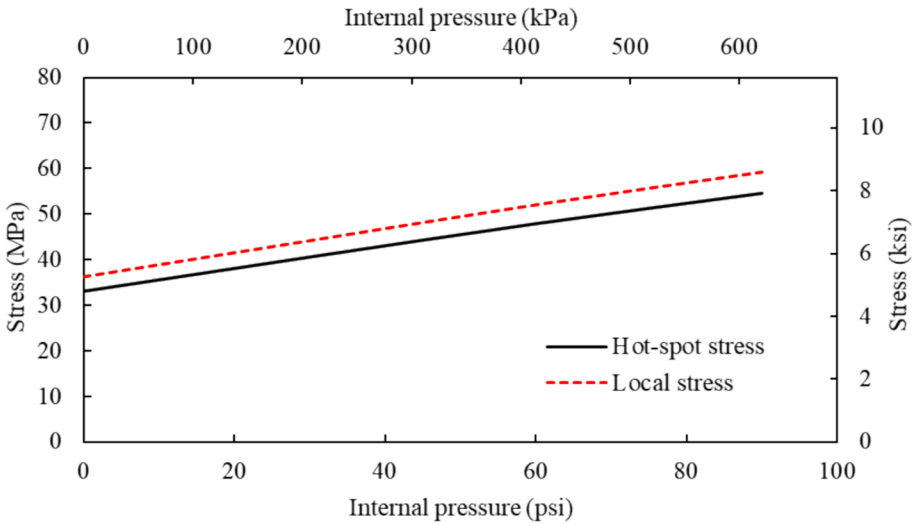

Fig. 7. A comparison of HSS and local stress in IRP at the discontinuity edge on the tension side.

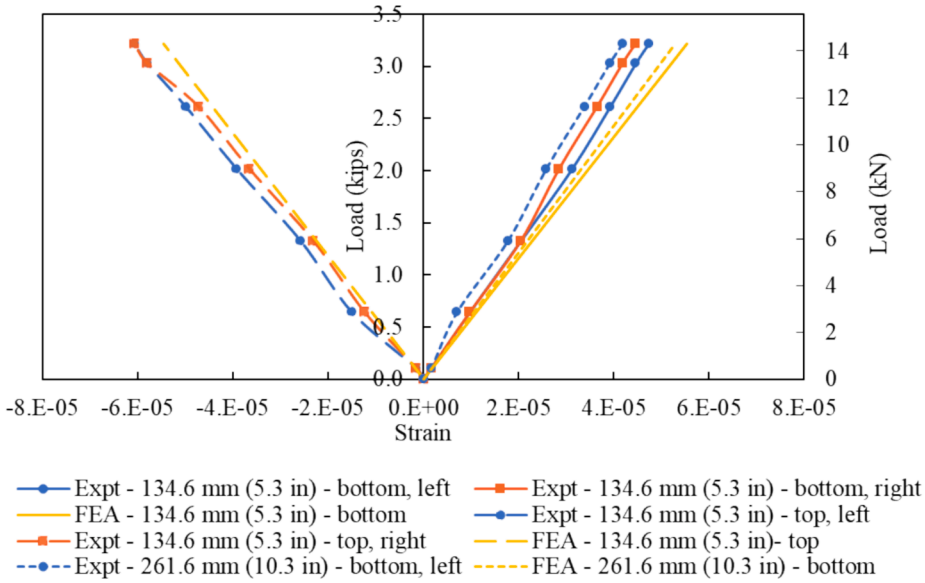

Fig. 8. Comparison of load–strain behaviours of IRP from FEA and laboratory experiments.

IRP system during bending are significantly lower than the axial stresses, as previously explained. The reason for this is that most IRP systems are designed to be stiffer and stronger in the circumferential than in the longitudinal directions. Hence, it is considered acceptable to neglect the analysis of fatigue life during bending based on the circumferential stresses. In subsequent analysis, the estimation of fatigue life is therefore based solely on the longitudinal stresses. According to the observed minimum fatigue lives, only the non-pressurized GFRP-1 out of four different scenarios examined, seems to be capable of meeting the design life requirement of one million loading cycles, while the systems with 206.8 kPa (30.0 psi) or higher are susceptible to failure well before reaching the intended service life. The fatigue damage contour plots reveal that, throughout its service life, the bottom of GFRP-1 IRP will undergo fatigue damage, with a damage factor greater than 1.0, exclusively at the discontinuity edges of host pipe segments when subjected to an internal pressure of 206.8 kPa (30.0 psi) as depicted in Fig. 13b (It is important to note that the damage value represents the ratio of the fatigue life of the IRP system to its intended design life of one million cycles). However, when exposed to an internal pressure of 413.7 kPa (60.0 psi) and 620.5 kPa (90.0 psi), even the bottom midspan of GFRP-1 will be susceptible to damage as shown in Fig. 13c and d. As the internal pressure rises, the damage to the lower portion of the IRP expands in its circumferential direction. Linear interpolation reveals that the GFRP-1 with thicknesses of 4.115 mm (0.162 in) and exposed to a transmitted traffic load of 14.8 kN (3.3 kips) will satisfy the design fatigue life if the internal pressure does not surpass 121.3 kPa (17.6 psi).

3.2. *Effect of internal pressure with different repair thickness*

The effect of internal pressure on critical stress (i.e. longitudinal tensile stress) and fatigue life for different repair thicknesses of GFRP-1 ranging from 3.175 mm (0.125 in) to 9.525 mm (0.375 in) under a transmitted traffic load of 14.8 kN (3.3 kips) is shown in Fig. 14a and b, respectively. According to Fig. 14a, under the same level of transmitted traffic loading, the critical stress in IRP with repair thicknesses of 3.175 mm (0.125 in), 6.35 mm (0.25 in) and 9.525 mm (0.375 in) increases linearly as the internal pressure rises, similar to that of IRP with 4.115 mm (0.162 in). This is because an increase in the internal pressure amplifies the force that causes IRP to elongate in the longitudinal direction. This results in an increase in internal pressure-induced

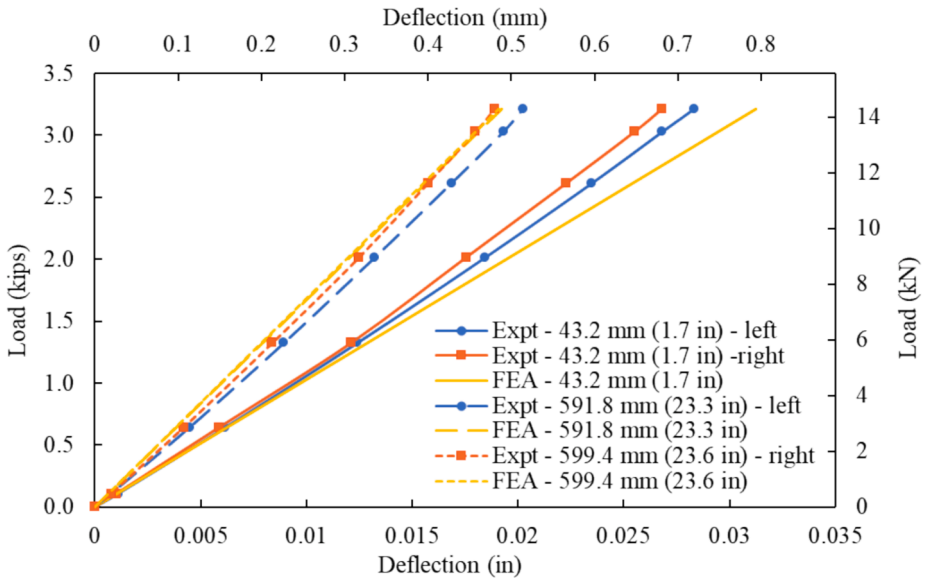

Fig. 9. Comparison of load–deflection behaviours of IRP from FEA and laboratory experiments.

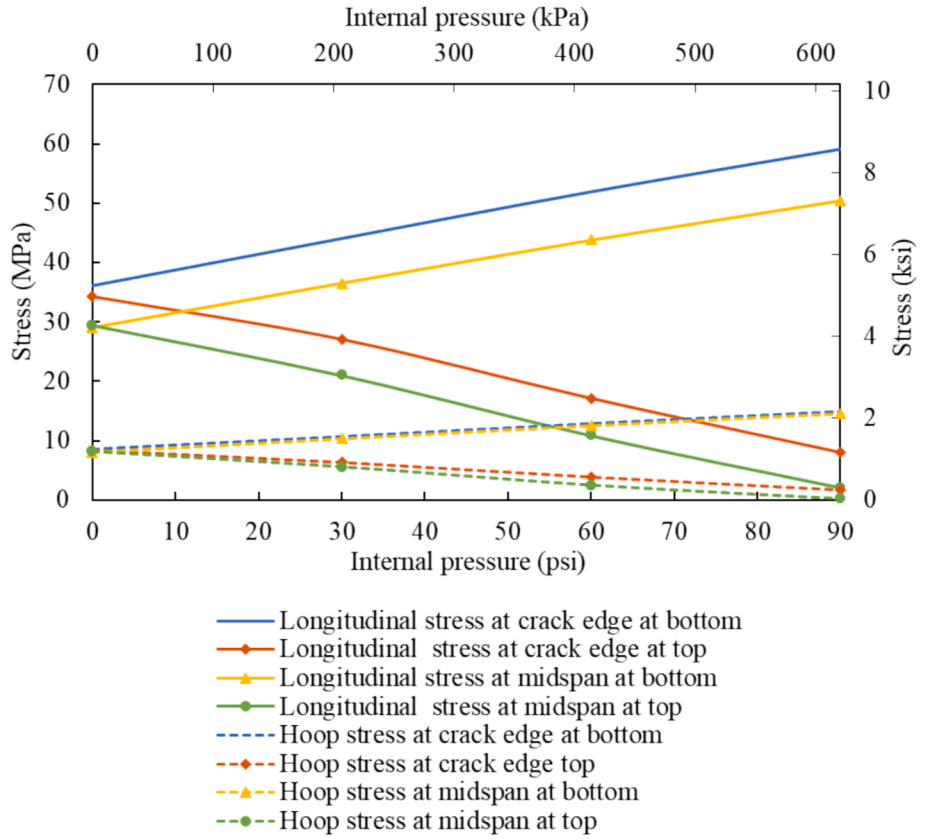

Fig. 10. Comparison between longitudinal stresses and circumferential stresses in IRP system with different internal pressures after undergoing cyclic bending.

longitudinal stress, which combines with the bending stress to produce the overall tensile stress in the longitudinal direction. Additionally, with an internal pressure of 620.5 kPa (90.0 psi), the maximal tensile stress generated in the IRP with thicknesses of 3.175 mm (0.125 in) and 9.525 mm (0.375 in) are respectively 62.3 % and 60.3 % higher than corresponding repair systems with no internal pressure. On the other hand, as the internal pressure rises, fatigue life exhibits a nonlinear decrease for all IRP thicknesses considered, even on a semi-log scale (Fig. 14b). Furthermore, while the 9.525 mm (0.375 in) thick IRP achieves the design life of one million cycles even with an internal pressure of 620.5 kPa (90.0 psi), the 3.175 mm (0.125 in) thick IRP is unable to meet the design requirement even without internal pressure. The IRP with thicknesses of 6.35 mm (0.25 in), on the other hand, cannot achieve one million cycles when the internal pressure exceeds 385.4 kPa (55.9 psi).

The influence of IRP thickness on the critical tensile stress in GFRP-1 under 14.8 kN (3.3 kips) of transmitted traffic load with multiple levels of internal pressure varying from zero to 620.5 kPa (90.0 psi) is depicted in Fig. 15a and b, respectively. As can be seen from Fig. 15a, the critical

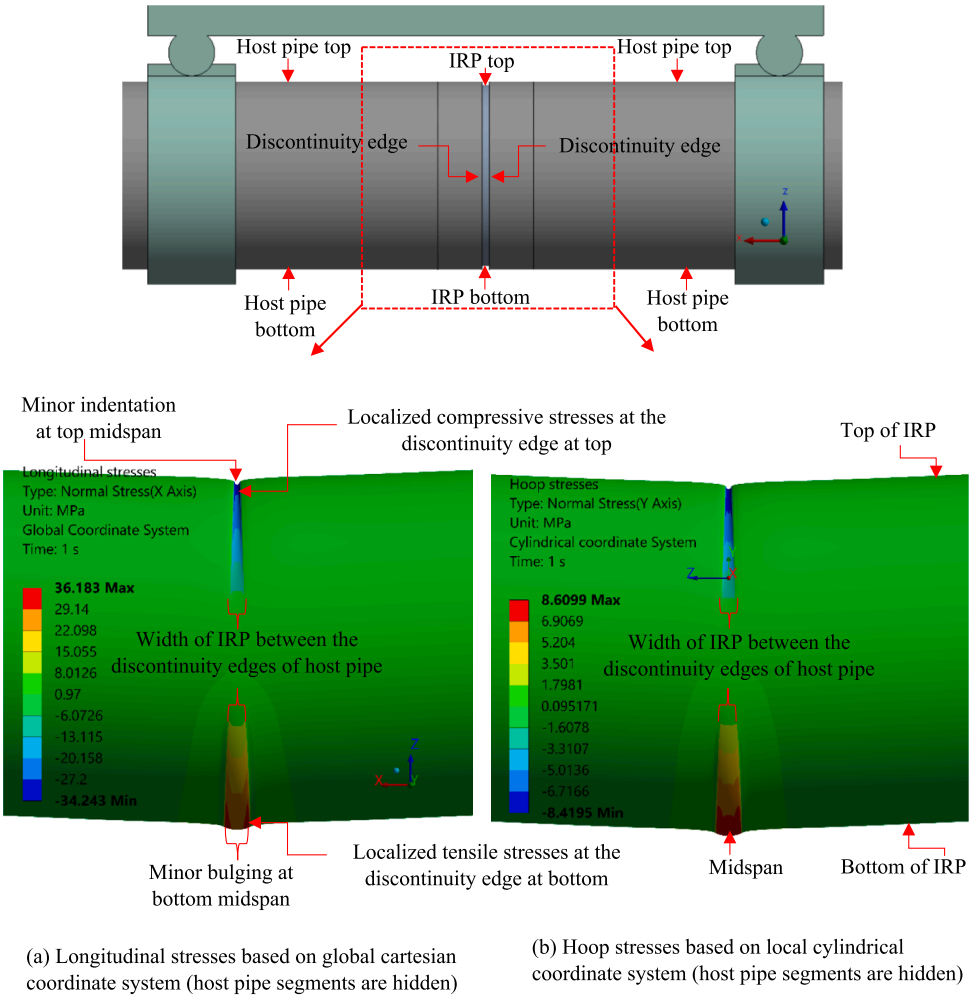

(a) Longitudinal stresses based on global cartesian coordinate system (host pipe segments are hidden)

(b) Hoop stresses based on local cylindrical coordinate system (host pipe segments are hidden)

Fig. 11. Contour plots of longitudinal and hoop stresses on the outer surface of non-pressurised IRP (mirrored results on symmetry planes).

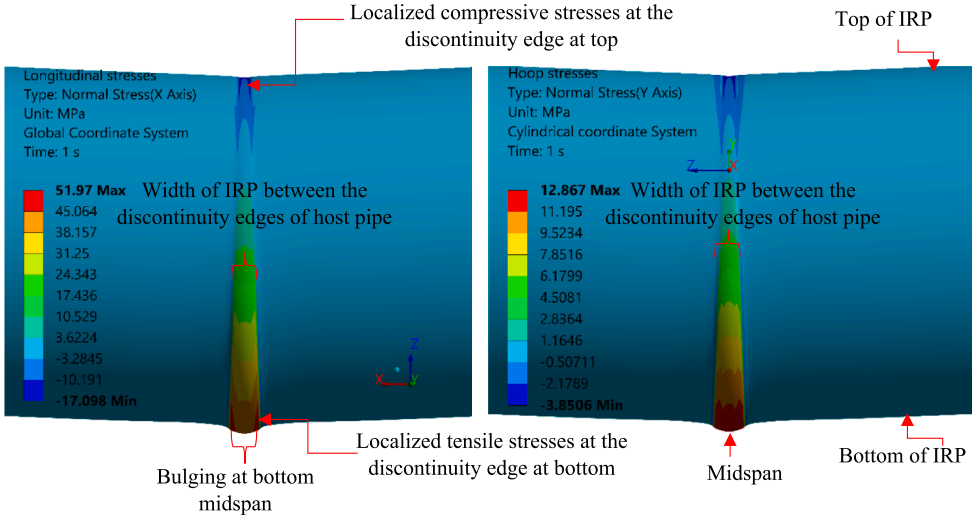

(a) Longitudinal stresses based on global cartesian coordinate system (host pipe segments are hidden)

(b) Hoop stresses based on local cylindrical coordinate system (host pipe segments are hidden)

Fig. 12. Contour plots of longitudinal and hoop stresses on the outer surface of pressurized IRP (413.7 kPa or 60.0 psi) (mirrored results on symmetry planes).

tensile stress decreases nonlinearly as the IRP thickness increases from 3.175 mm (0.125 in) to 9.525 mm (0.375 in) for all the internal pressures considered. This is because the increasing IRP thickness can distribute the combined forces induced by both bending and internal pressure more evenly across the cross-section. Additionally, thicker IRP also has greater bending and axial stiffness, which enables it to resist

Table 3
Fatigue life comparison between the circumferential and longitudinal stresses.

Internal pressure	Fatigue life (cycles)	
	Based on maximum alternating stress in longitudinal direction and corresponding S-N behaviour (MOE of 3.739 GPa or 542 ksi)	Based on maximum alternating stress in circumferential direction and corresponding S-N behaviour (MOE of 9.7 GPa or 1407 ksi)
zero	2.7E+06	≫1.0E+09
206.8 kPa (30.0 psi)	1.2E+05	≫1.0E+09
413.7 kPa (60.0 psi)	8492	≫1.0E+09
620.5 kPa (90.0 psi)	869	≫1.0E+09

deformation and strain under combined loading. This also results in lower stress concentration at the discontinuity edge, as thicker IRP can better withstand the loading condition without experiencing excessive deformation. The greatest stress reduction (45.5%) occurs when the repair thickness increases under the highest internal pressure (620.5 kPa or 90.0 psi), while the lowest reduction (44.9%) is observed when there is no internal pressure in the system. However, as shown in Fig. 15b, the fatigue life exhibits a nonlinear increase, even on a semi-log scale, as the repair thickness increases from 3.175 mm (0.125 in) to 9.525 mm (0.375 in) under all the internal pressures. When subjected to the transmitted traffic load of 14.8 kN (3.3 kips), in order to satisfy the design fatigue life criteria at an internal pressure level of zero, 206.8 kPa (30.0 psi), 413.7 kPa (60.0 psi) and 620.5 kPa (90.0 psi), the minimum required IRP thicknesses should be 3.7 mm (0.15 in), 5.3 mm (0.21 in), 7.1 mm (0.28 in) and 8.9 mm (0.35 in), respectively. Therefore, the minimum IRP thickness necessary to meet the design life requirement with an internal pressure of 620.5 kPa (90.0 psi) is 2.4 times greater than that required for a non-pressurized state.

3.3. *Effect of internal pressure with different MOEs of IRP materials*

Fig. 16 compares the effect of MOE on the critical tensile strain of 4.115 mm (0.162 in) thick IRP for different levels of internal pressure under the transmitted traffic load of 14.8 kN (3.3 kips). Regardless of the level of internal pressure, the strain undergoes a dramatic nonlinear decrease when the MOE increases from 1.744 GPa (253 ksi) to 7.9 (1146 ksi), followed by a gradual reduction until it reaches a MOE of 38.63 GPa (5603 ksi). The reduction in strain with increasing MOE is consistent

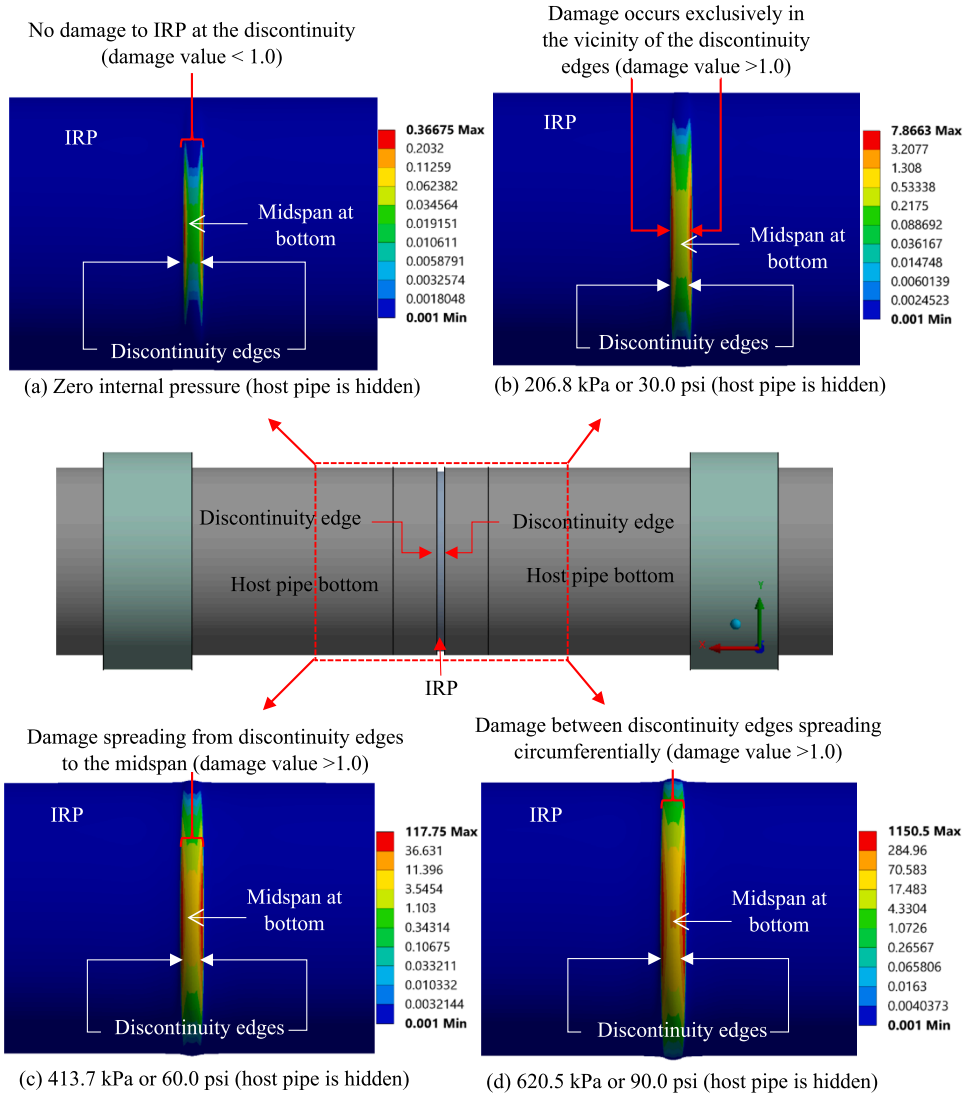

Fig. 13. Contour plots of fatigue damage on the bottom midspan of pressurized and non-pressurized GFRP-1 IRPs during their service life (To facilitate clear visualisation, host pipe segments are hidden).

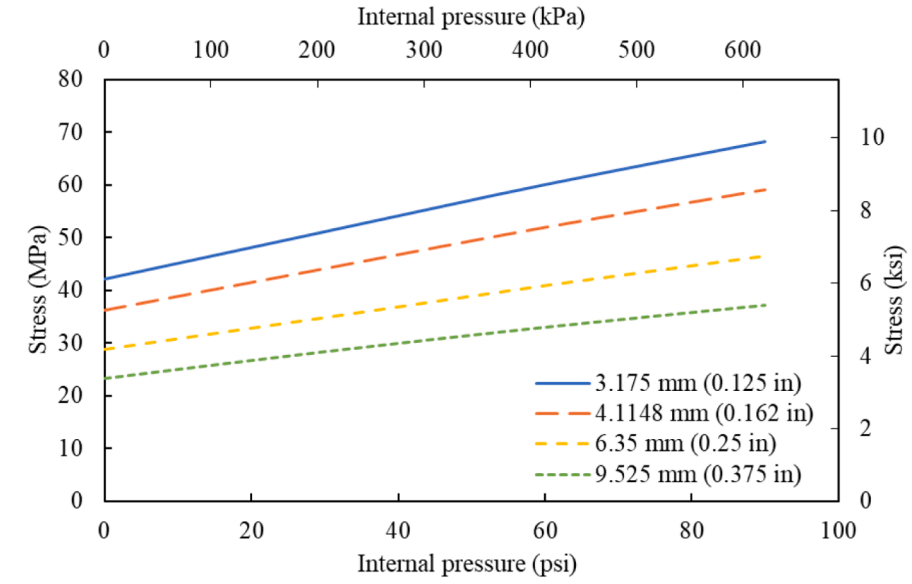

(a)

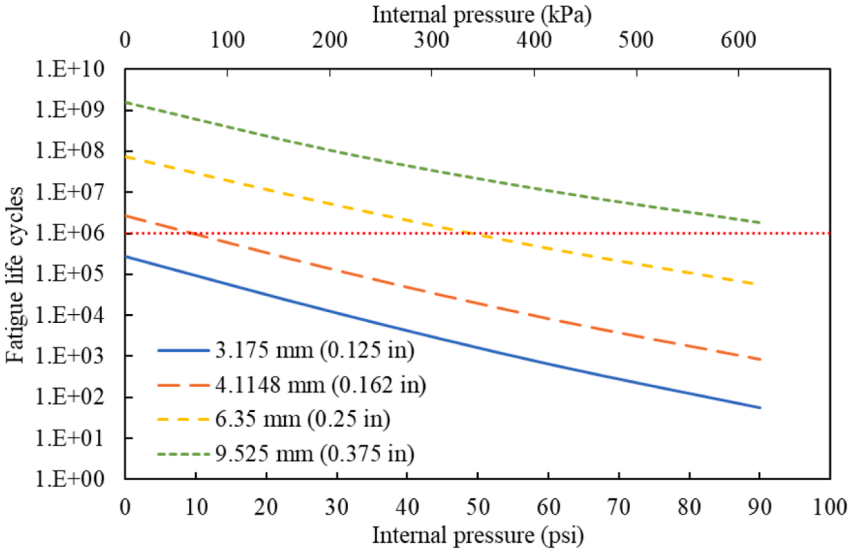

(b)

Fig. 14. Effect of internal pressure on (a) critical tensile stress and (b) minimum fatigue life of IRP repair systems with different repair thickness.

across all the internal pressure levels, with an overall reduction of 96.7%. When the MOE of IRP is at or below 2.4 GPa (348 ksi), 2.9 GPa (421 ksi) and 3.2 GPa (464 ksi), respectively, the critical strain surpasses the design strain limitation of 0.02 at internal pressures of 206.8 kPa (30.0 psi), 413.7 kPa (60.0 psi) and 620.5 kPa (90.0 psi). Fig. 17 displays the response of critical stress of IRP with different levels of internal pressure as the MOE increases under a transmitted traffic loading of 14.8 kN (3.3 kips). The graph indicates that the critical stress remains almost constant at all internal pressures as the MOE of IRP increases from 1.744 GPa to around 15 GPa (2176 ksi). However, from 15 GPa (2176 ksi) up to 30 GPa (4351 ksi) of MOE, the critical stress produced in the IRP without internal pressure and internal pressures of 206.8 kPa (30.0 psi) and 413.7 kPa (60.0 psi) nonlinearly decreases in a concave up manner, after which it remains stable until MOE of 38.63 GPa (5603 ksi). On the other hand, the critical stress generated in the IRP with the internal pressure of 620.5 kPa (90.0 psi) decreases nonlinearly in a concave-down manner as MOE increases from 15 GPa (2176 ksi) to 38.63 GPa (5603 ksi). The reduction in stress is attributed to the fact that the MOE is directly related to the stiffness or its ability to resist deformation under stress. When a stiffer IRP is used, it can more effectively distribute the load and resist deformation under the combined effect of internal pressure and transmitted traffic load than a more flexible IRP. As a result, the concentration of stress at the discontinuity edge diminishes, resulting in a reduction of maximum tensile stress.

Table 4 illustrates the fatigue life of IRP with different levels of internal pressures subjected to a transmitted traffic loading of 14.8 kN (3.3 kips) with varying MOE. It is evident that the IRP with MOE of 1.744 GPa (253 ksi), 3.739 GPa (542 ksi), and 7.9 GPa (1146 ksi) exhibits a significant increase in fatigue life as the internal pressure is raised from zero to 620.5 kPa (90.0 psi). Among all the material systems evaluated, the polymeric IRP, which has the lowest MOE demonstrates the shortest fatigue life across all the internal pressure levels. The polymeric IRP lasts

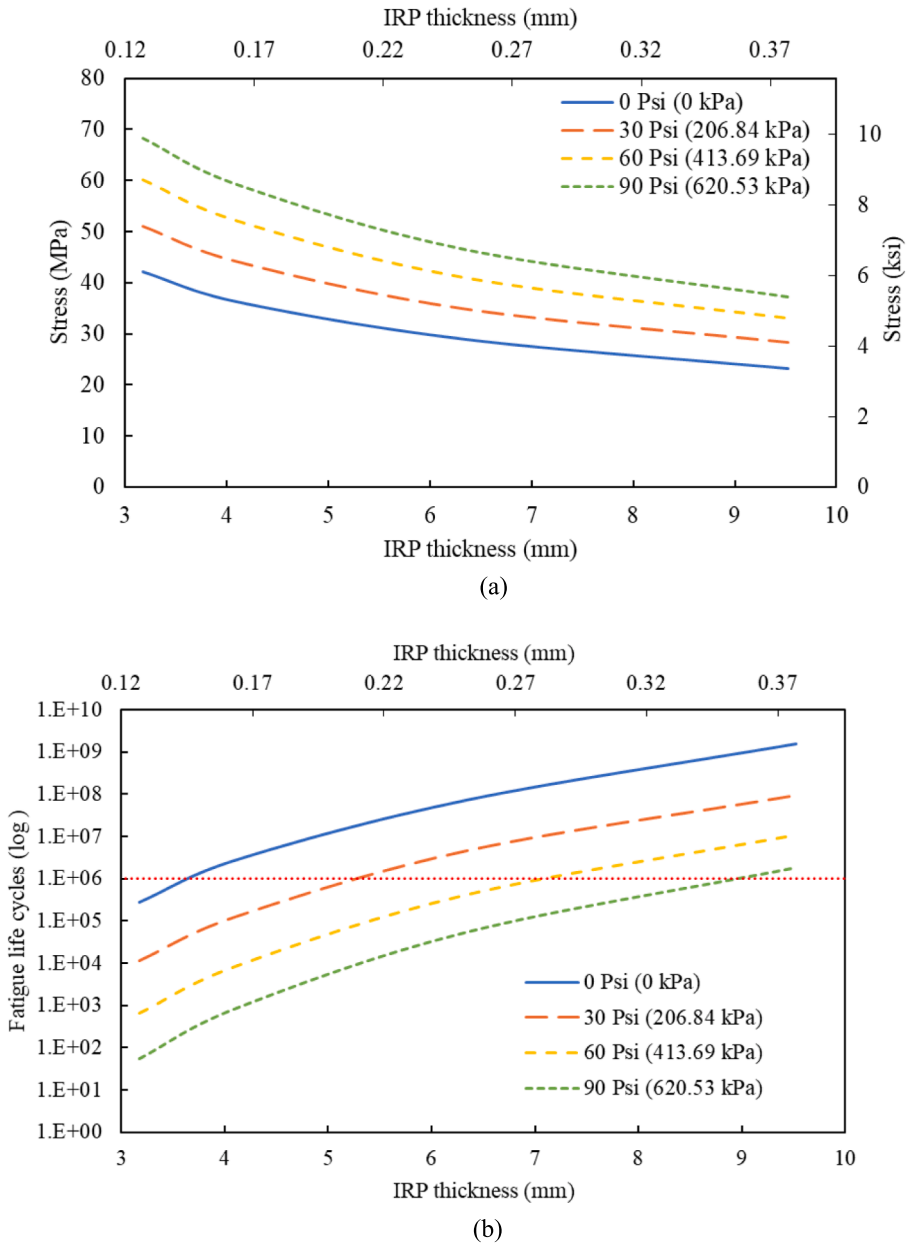

Fig. 15. Effect of IRP thickness on (a) critical tensile stress and (b) minimum fatigue life of IRP systems with different internal pressure.

only 130 cycles and one cycle under conditions of zero internal pressure and internal pressure of 206.8 kPa (30.0 psi), respectively. However, when the polymeric IRPs are exposed to an internal pressure of 413.7 kPa (60.0 psi) or above, they fail before even completing a single cycle because the alternating stress levels are too high compared to the maximum limit specified in the S-N curve. When the MOE of IRP is 7.9 (1146 ksi) or higher, the design life requirement is met even at the highest internal pressure under consideration. Furthermore, to satisfy the design life criterion under internal pressures of zero, 206.8 kPa (30.0 psi), 413.7 kPa (60.0 psi) and 620.5 kPa (90.0 psi), it is necessary for MOE of IRP with a thickness of 4.115 mm (0.162 in) to be 3.5 GPa (508 ksi), 4.2 GPa (609 ksi), 4.8 GPa (696 ksi) and 5.3 GPa (769 ksi), correspondingly (using liner interpolation).

3.4. Effect of internal pressure with different loading levels transmitted from vehicular traffic

The influence of internal pressure on critical tensile stress and fatigue life of a 4.115 mm (0.162 in) thick GFRP-1 under different levels of transmitted traffic loads is shown in Fig. 18a and b, respectively. As per Fig. 18a, critical stress in IRP increases linearly with the rise in internal pressure for transmitted traffic loads of 10.0 kN (2.2 kips), 20.0 kN (4.5 kips) and 25.0 kN (5.6 kips), similar to the behaviour observed under the transmitted traffic load of 14.8 kN. It should be noted, however, that the design strain limit of 0.02 is exceeded by the repair systems with the internal pressure of 620.5 kPa (90.0 psi) when subjected to a transmitted traffic load of 25.0 kN (5.6 kips). In comparison to the non-pressurized system, the overall increase in maximal tensile stresses in IRP at 620.5 kPa (90.0 psi) under transmitted traffic loads of 10.0 kN (2.2 kips), 14.8 kN (3.3 kips), 20.0 kN (4.5 kips) and 25.0 kN (5.6 kips) are 88.6%, 62.1, 47.8% and 38.7%, respectively. This suggests that an increase in internal pressure leads to a more pronounced impact on repair systems that are exposed to comparably lower transmitted traffic loads. This is because, in comparison to the contribution of the bending stress induced by the transmitted traffic load, the longitudinal stress component produced by internal pressure makes a substantial contribution to the resultant

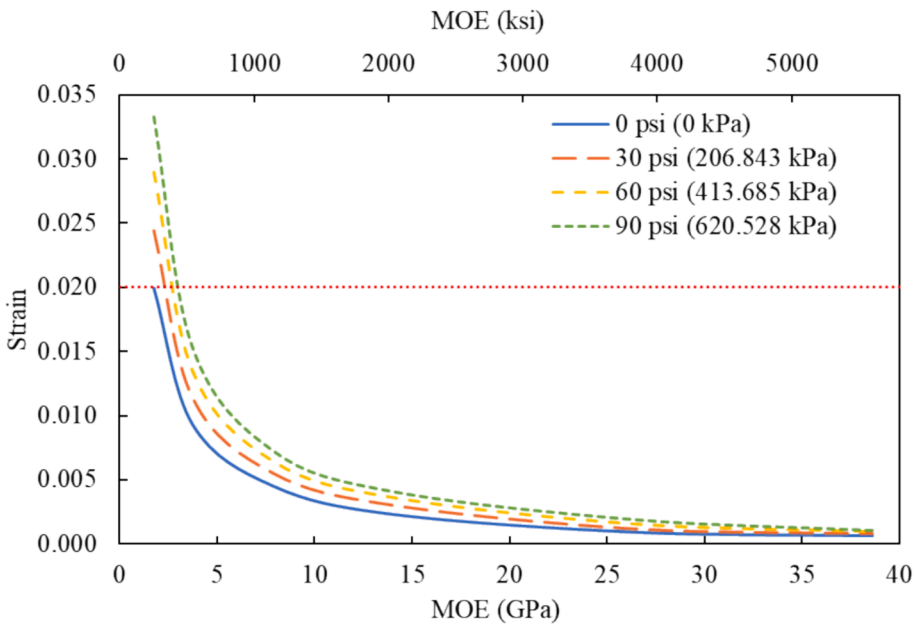

Fig. 16. Effect of MOE on the critical tensile strain of IRP with different internal pressure.

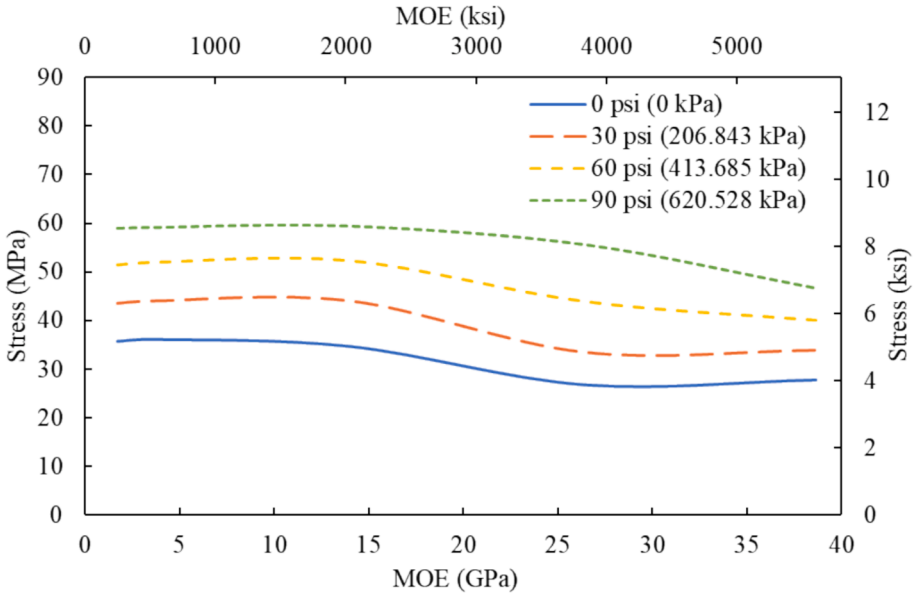

Fig. 17. Effect of MOE on critical stress in 4.115 mm (0.162 in) thick IRP with different internal pressure.

Table 4
Minimum fatigue life of 4.115 mm (0.162 in) thick IRP with different MOE and levels of internal pressure.

Internal pressure	Fatigue life cycles					
	1.744 GPa (253 ksi) [Polymer]	3.739 GPa (542 ksi) [GFRP-1]	7.9 (1146 ksi) [GFRP-2]	14.03 GPa (2035 ksi) [GFRP-3]	26.43 GPa (3833 ksi) [GFRP-4]	38.63 GPa (5603 ksi) [GFRP-5]
zero	130	2.7E+06	3.0E+11	≫1E+12	≫1E+12	≫1E+12
206.8 kPa (30.0 psi)	1	1.2E+05	5.2E+10	≫1E+12	≫1E+12	≫1E+12
413.7 kPa (60.0 psi)	0	8492	1.3E+10	≫1E+12	≫1E+12	≫1E+12
620.5 kPa (90.0 psi)	0	869	4.13E+09	≫1E+12	≫1E+12	≫1E+12

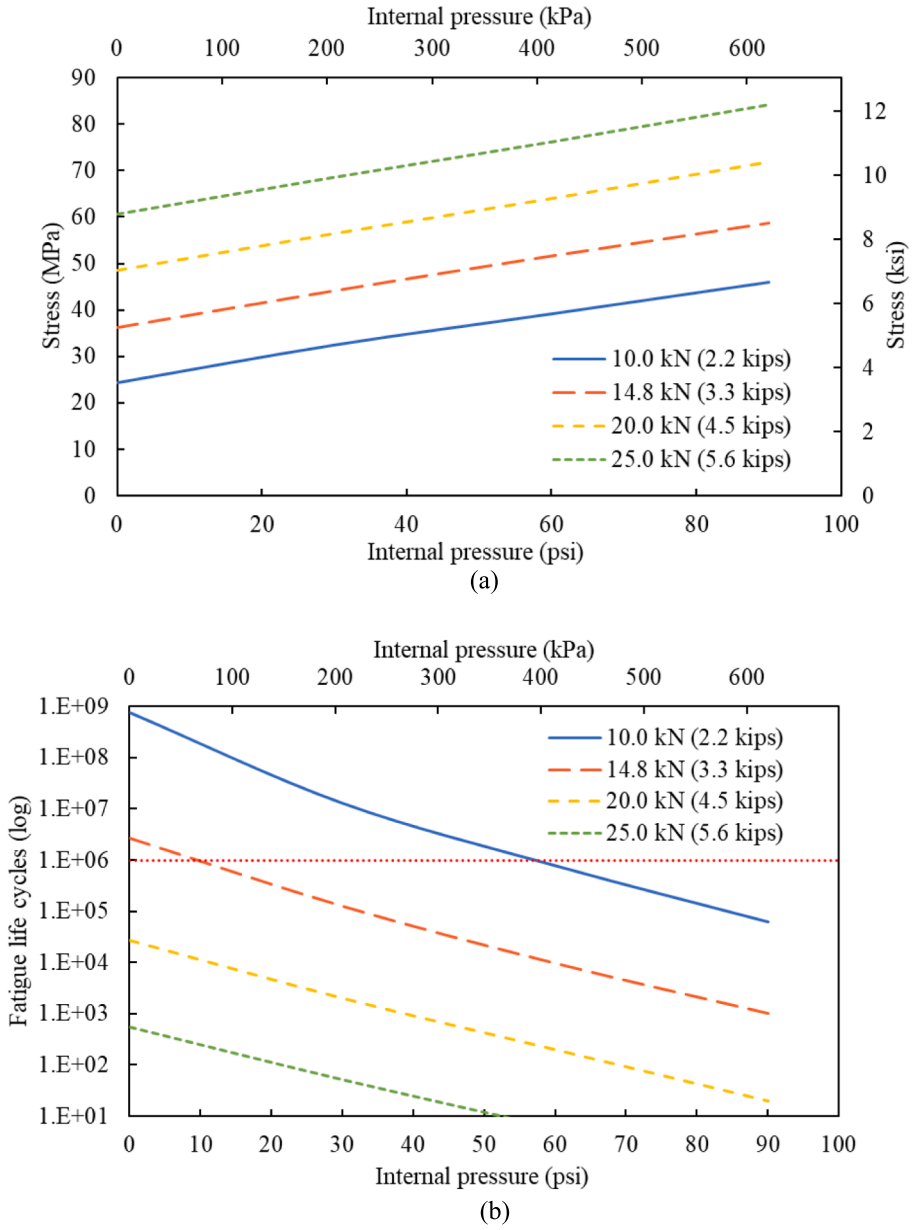

Fig. 18. Effect of internal pressure on (a) critical tensile stress and (b) minimum fatigue life of IRP systems exposed to different levels of loads transmitted from vehicular traffic.

longitudinal tensile stress. As illustrated in Fig. 18b, the fatigue life of IRP subjected to the transmitted traffic load of 10.0 kN (2.2 kips) decreases nonlinearly with increasing internal pressure from zero to 620.5 kPa (90.0 psi), which is similar to the behaviour when subjected to a load of 14.8 kN, whereas those under 20.0 kN (4.5 kips) or higher decrease almost linearly. The IRP subjected to transmitted traffic loads of 10.0 kN (2.2 kips) exceeds one million cycles when the internal pressure is lower than 389.6 kPa (56.5 psi). However, IRPs exposed to transmitted traffic loads of 20.0 kN (4.5 kips) or greater are unable to meet the design life requirement, even in the absence of internal pressure.

Fig. 19a and b show the effect of transmitted traffic load on the critical tensile stress and service life of GFRP-1IRP with a thickness of 4.115 mm (0.162 in) under various levels of internal pressure ranging from zero to 620.5 kPa (90.0 psi). As can be seen from Fig. 19a, the critical tensile stresses experienced by non-pressurized, and all pressurized IRPs increase almost linearly as the transmitted traffic load rises from 5.0 kN (1.1 kips) to 25.0 kN (5.6 kips). The corresponding percentage increases in critical tensile stresses at an internal pressure of zero, 206.8 kPa (30.0 psi), 413.7 kPa (60.0 psi) and 620.5 kPa (90.0 psi) are 523.1%, 244.9%, 189.9% and 149.8%, respectively. This is because an increasing transmitted traffic load causes a greater deformation of the IRP, which leads to a more pronounced change in stress distribution and a greater concentration of stress at the discontinuity edge. Additionally, compared to the system without internal pressure, the presence of internal pressure causes the IRP to expand, which can further change stress distribution and increase stress concentration at the discontinuity edge. Fig. 19b demonstrates that the fatigue lives of IRP, both with and without internal pressure, exhibit a slight nonlinear decrease as the transmitted traffic load is increased, even when represented on a semi-log scale. The IRP with a thickness of 4.115 mm (0.162 in) operating at zero, 206.8 kPa (30.0 psi), 413.7 kPa (60.0 psi) and 620.5 kPa (90.0 psi) internal pressure can only satisfy the design fatigue life criteria if the transmitted traffic load level remains below 15.8 kN (3.6 kips), 12.4 kN (2.8 kips), 9.7 kN (2.2 kips) and 6.7 kN (1.5 kips), respectively.

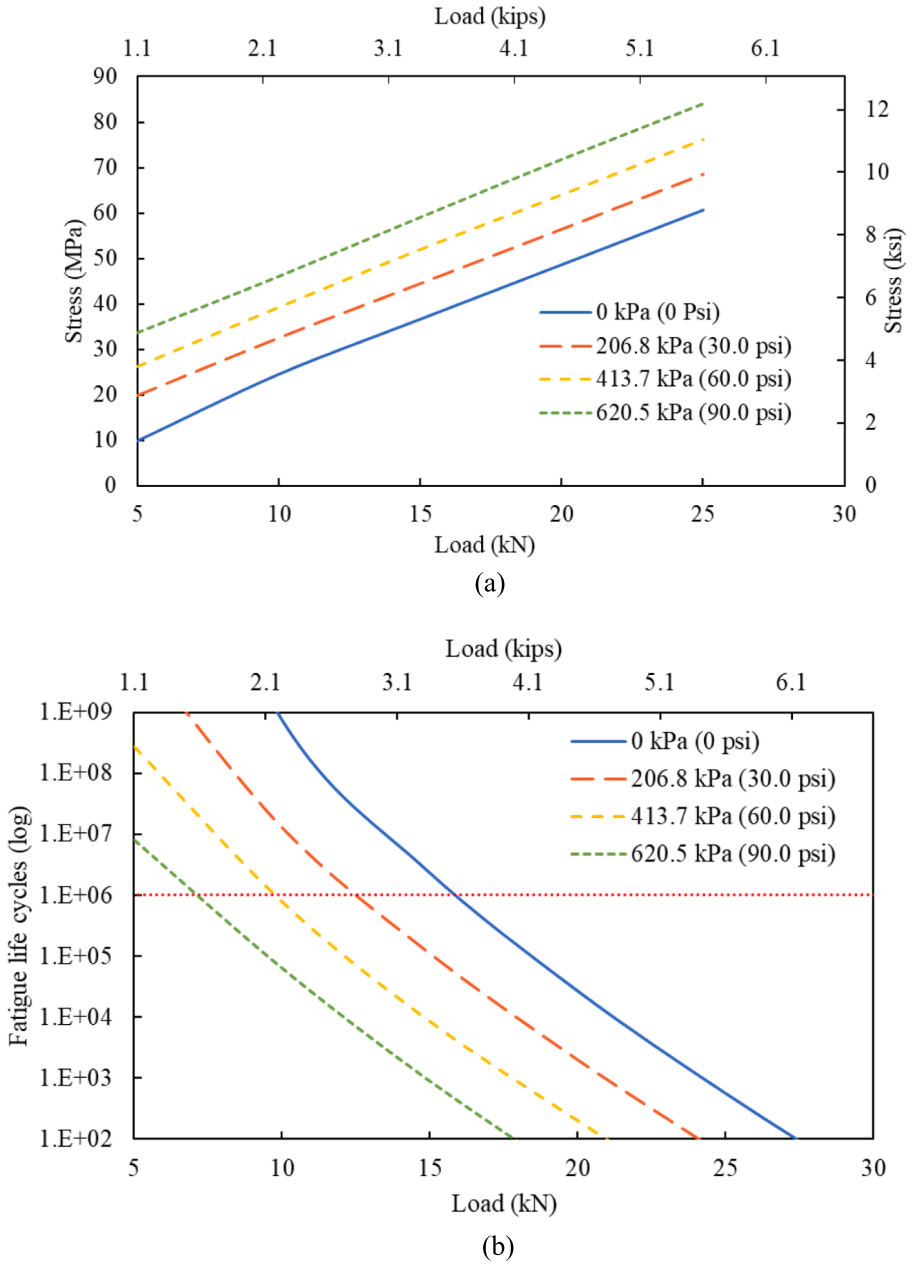

Fig. 19. Effect of transmitted traffic load level on (a) critical tensile stress and (b) minimum fatigue life of IRP with different levels of internal pressure.

3.5. Mathematical expressions for fatigue life prediction of IRP systems

Two mathematical formulae were developed to predict the fatigue life and strain of an IRP under the combined effect of internal pressure and transmitted traffic load. The formulae are established based on the FEA results obtained from a comprehensive parametric study, with the aim of facilitating efficient design practice. The purpose of formulating an equation for estimating strain is to ensure that the IRP system is within the designated strain limit of 0.02 prior to conducting predictions of fatigue life, which will be elaborated on subsequently. Both equations contain four independent variables, namely, MOE and thickness of IRP, transmitted traffic load, and internal pressure. The selection of the MOE range, from 1.744 GPa (253 ksi) to 7.9 (1146 ksi), is based on finite fatigue life observation obtained from the parametric study. The repair thicknesses and internal pressures employed are in accordance with the ones detailed in section 2.1. However, the scope of the transmitted traffic load, as described in section 2.1, has been expanded to cover a wide range of data. The expanded transmitted traffic load ranges from 5.0 kN (1.1 kips) to 40.0 kN (9.0 kips). To ensure consistent and standardised comparison across different scales and to facilitate meaningful analysis and interpretation of data, the effect of distinct scales or units presented in variables is eliminated. This is accomplished by dividing both independent and dependent variables by their respective referenced values while ensuring consistency in units before model fitting and equation derivation. Through this process, dimensionless quantities are obtained, thereby ensuring normalisation and enhancing the validity of the derived equations.

The mathematical formulations were derived by fitting the FEA dataset into parameterized user-defined functions using the nonlinear least square curve fitting method. This was accomplished using the lsqcurvefit solver, which is available in the MATLAB optimization toolbox. The lsqcurvefit solver starts by using initial guesses and determines the coefficients that provide the best fit for the nonlinear function to the given dataset, using the least-square approach. This can

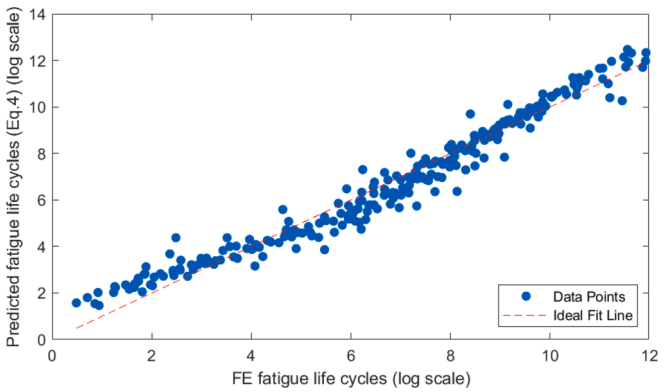

Fig. 20. A comparison between FE and predicted fatigue life cycles on a logarithmic scale.

be represented by Eq. (1), where *fun* represents the function used for fitting, x represents the coefficients of the function, x_0 represents the initial guesses for the coefficients, *xdata* represents the independent variables, and *ydata* represents the dependent variables.

$$x = lsqcurvefit(fun, x_0, xdata, ydata) \tag{1}$$

The user-defined nonlinear functions that are employed to fit the models where the dependent variable is fatigue life cycles (N) and strain (ε) are respectively as Eq. (2) and Eq. (3). In these equations, E represents the MOE of repair material in MPa, t is the repair thickness in mm, F is the load transmitted from vehicular traffic in N, and p is the internal pressure in MPa. The referenced values for MOE, repair thickness, transmitted traffic load, internal pressure, fatigue life cycles, and strain are denoted by E_{ref}, t_{ref}, F_{ref}, p_{ref}, N_{ref}, and ε_{ref}, respectively. The model equations for fatigue life cycles and strain are characterized by eight unknown dimensionless coefficients, denoted as $\alpha_1 - \alpha_8$ for the former, and as $\beta_1 - \beta_8$ for the latter.

$$\frac{\log_{10}(N)}{\log_{10}(N_{ref})} = \alpha_1\left(\frac{E}{E_{ref}}\right)^{\alpha_2} + \alpha_3\left(\frac{t}{t_{ref}}\right)^{\alpha_4} + \alpha_5\left(\frac{F}{F_{ref}}\right)^{\alpha_6} + \alpha_7\left(\frac{p}{p_{ref}}\right)^{\alpha_8} \tag{2}$$

$$\frac{\varepsilon}{\varepsilon_{ref}} = \beta_1\left(\frac{E}{E_{ref}}\right)^{\beta_2} + \beta_3\left(\frac{t}{t_{ref}}\right)^{\beta_4} + \beta_5\left(\frac{F}{F_{ref}}\right)^{\beta_6} + \beta_7\left(\frac{p}{p_{ref}}\right)^{\beta_8} \tag{3}$$

where,

- E_{ref} = 3739 MPa(MOE of GFRP-1 IRP material)
- t_{ref} = 4.115 mm
- F_{ref} = 14800 N(Transmitted traffic load)
- p_{ref} = 0.414 MPa(Operating internal pressure)
- N_{ref} = 10^6(Design life)
- ε_{ref} = 0.02(Design strain limit)

Following the process of model fitting, the mathematical expressions for predicting the fatigue life (as expressed on a logarithmic scale) and strain of IRP were derived as shown in Eq. (4) and Eq. (5), respectively. In order to assess the validity of the predictive capabilities of the derived Eqs. (4) and (5), a comparison was conducted between the predicted fatigue life and strain responses and corresponding FEA counterparts, as illustrated in Fig. 20 and Fig. 21, respectively. The comparisons indicate a favourable level of agreement between the FE responses and predicted responses for both fatigue life and strain, with only minor deviations, confirming the robustness of the proposed equations. The R-squared values of Eqs. (4) and (5) are determined to be 0.96 and 0.95, respectively, demonstrating a strong correlation between predicted and FE responses for both fatigue life and strain. In addition, the root means square error (RMSE) and mean absolute error (MAE) of Eq. (4) are both found to be 0.4, whereas those of Eq. (5) are computed to be 0.001, showing a relatively close fit between the predicted and FEA responses. Overall, according to the comparison of actual and predicted responses and evaluated metrics, the generated Eqs. (4) and (5) can be considered to have satisfactory accuracy and predictive capabilities.

$$\log_{10}(N) = 6\left(0.79\left(\frac{E}{3700}\right)^{1.15} + 5.07\left(\frac{t}{4.1}\right)^{0.09} - 5.01\left(\frac{F}{14800}\right)^{0.13} - 0.2\left(\frac{p}{0.4}\right)^{1.1}\right) \tag{4}$$

$$\varepsilon = 0.02\left(-7.6\left(\frac{E}{3700}\right)^{0.07} + 7.22\left(\frac{t}{4.1}\right)^{-0.04} + 0.95\left(\frac{F}{14800}\right)^{0.35} + 0.12\left(\frac{p}{0.4}\right)^{1.06}\right) \tag{5}$$

To facilitate the application of the derived formulations for generating design charts for the fatigue life of IRP systems, a MATLAB function was developed. The function enables the user to input the desired transmitted traffic load and internal pressure. It then calculates the maximum strain of the IRP system by utilizing Eq. (5) over a specified range of MOEs and thicknesses of the repair materials. Eq. (5) is constrained to

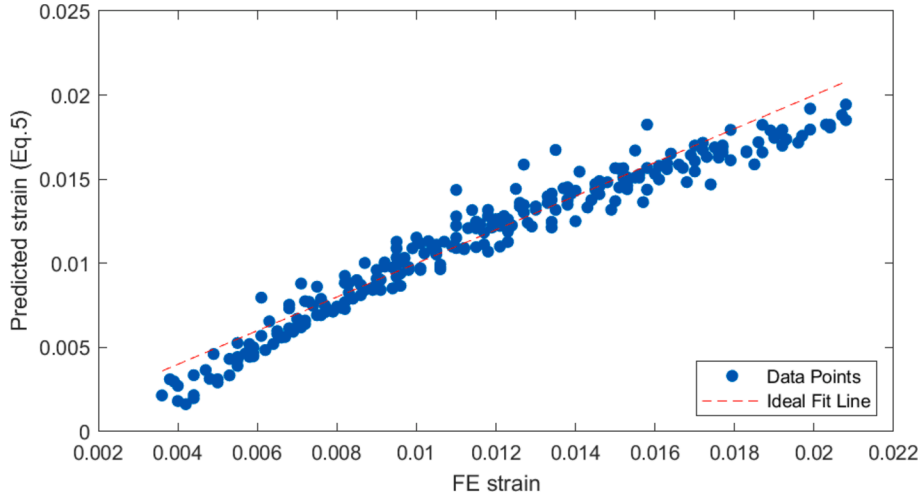

Fig. 21. A comparison between FE and predicted strain.

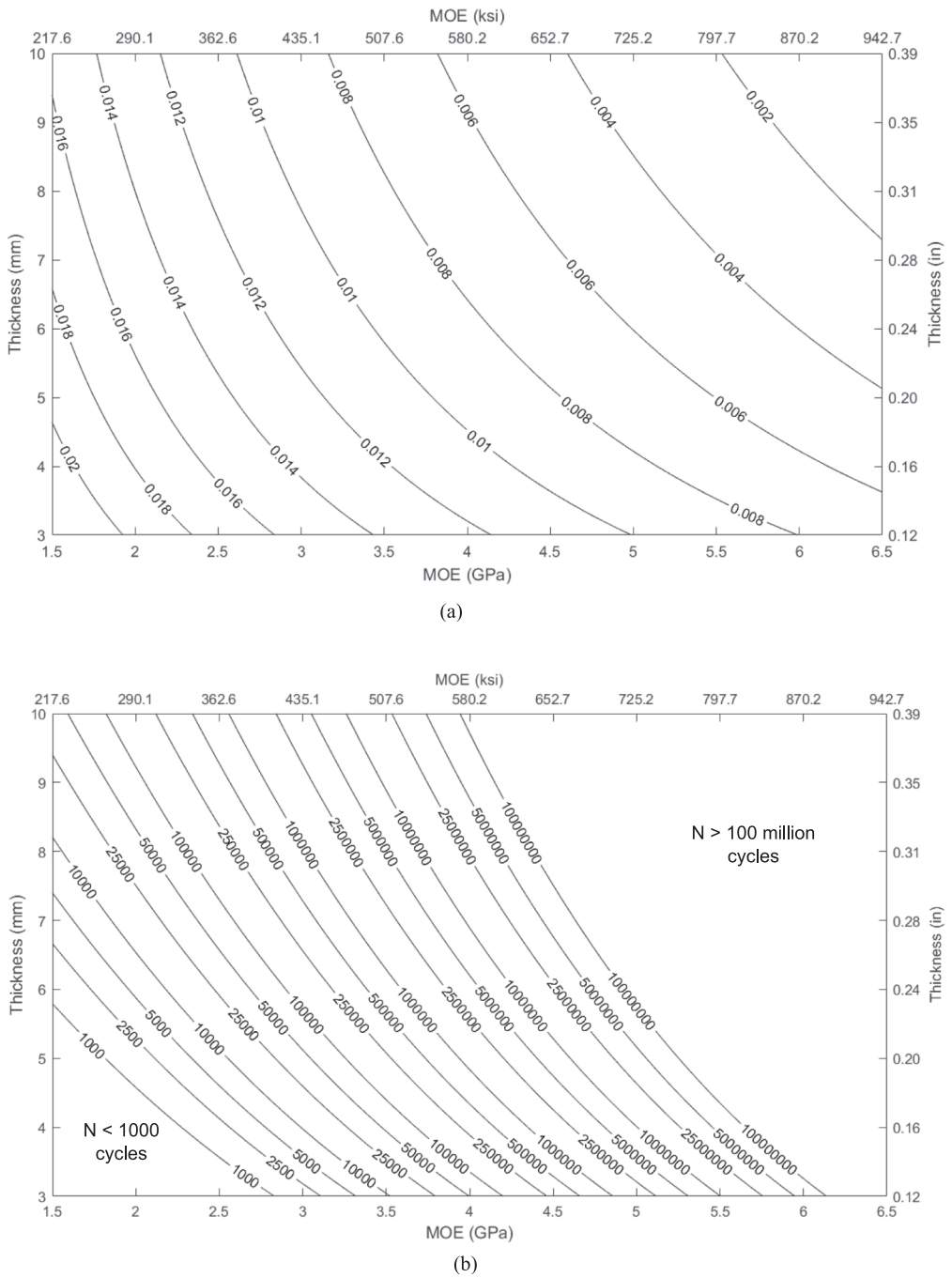

Fig. 22. (a) Strain and (b) fatigue life responses for varying MOE and thickness subjected to transmitted traffic load of 14.8 kN (3.3 kips) under zero internal pressure.

ensure that it predicts the strain values within the design strain limit of 0.02. The function then extracts all possible combinations of MOE of IRP materials and IRP thickness that satisfy the design strain criteria, given a user-defined transmitted traffic load and internal pressure. The extracted parameters are subsequently applied to Eq. (4) to estimate the corresponding fatigue life cycles and generate a graphical representation of fatigue lives in the form of a contour plot for various combinations of MOE and IRP thicknesses. The predicted fatigue lives shown on the contour plots are limited to a minimum of 1000 cycles and a maximum of 100 million cycles. This MATLAB function enables users to input relevant parameters interactively and generate fatigue life plots, thereby exploring various combinations of MOE and IRP thicknesses that meet the desired service life. This feature facilitates engineers and designers to make informed decisions for selecting design parameters that meet the intended design life requirement. Employing the developed MATLAB function, the obtained fatigue life contour plots for varying MOE and thickness exposed to a transmitted traffic load of 14.8 kN (3.3 kips) under internal pressures of zero, 206.8 kPa (30.0 psi), 413.7 kPa (60.0 psi) and 620.5 kPa (90.0 psi) are shown in Fig. 22–25, respectively.

4. Conclusion

This study presents a process to numerically investigate the fatigue performance of fully bonded internal replacement pipe (IRP) systems used for the trenchless rehabilitation of discontinuous legacy pipelines under the combined effect of transmitted traffic loading and internal

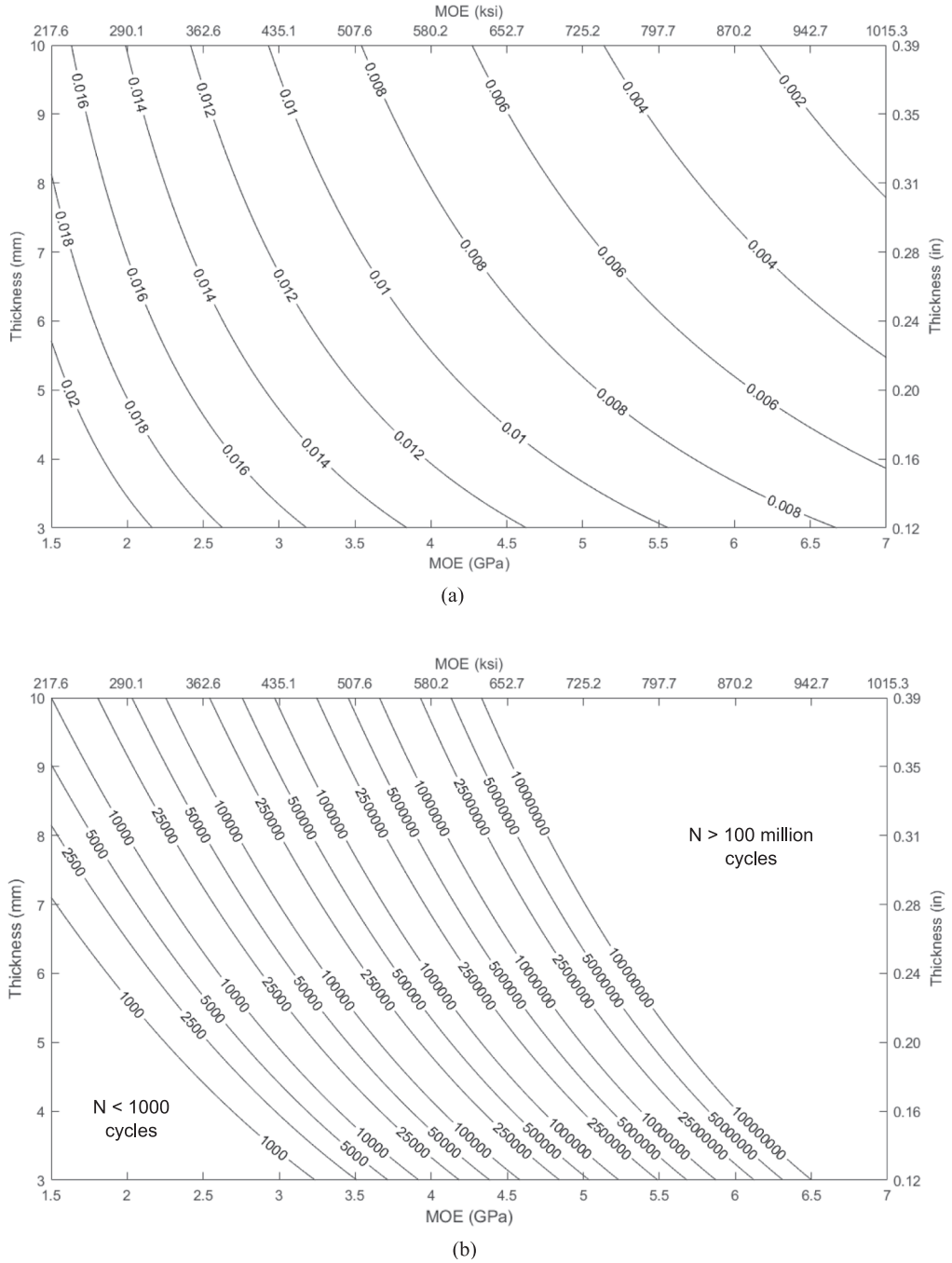

Fig. 23. (a) Strain and (b) fatigue life responses for varying MOE and thickness subjected to a transmitted traffic load of 14.8 kN (3.3 kips) under internal pressure of 206.8 kPa (30.0 psi).

pressure. The influence of thickness and modulus of elasticity (MOE) of the IRP, the magnitude of transmitted traffic load and the level of internal pressure on the fatigue performance were also analysed. The present study required simplifications for effective fatigue analysis under a variety of internal pressures and external load levels. This work assumed that the IRP remained fully bonded to the host pipe throughout fatigue loading, which is an important simplification but one that represents a worst-case scenario for the induced stress levels. The material assumptions included: linear elastic isotropic materials, failure strains of 0.02, and S-N curves developed from literature and limited experimental data. The use of the local stress opposed to the more rigorous HSS is justified. Future work to investigate these various aspects and expand on the presented methodology is encouraged. Considering these aforementioned simplifications, the following conclusions can be drawn from the outcomes of this study:

- The rise in the internal pressure increases the longitudinal and hoop stresses in the invert of IRP, which is under tension due to bending but decreases the stresses in the crown of IRP, which is under compression.
- Longitudinal stresses during bending are significantly greater than hoop stress at any location along IRP, regardless of the magnitude of internal pressure.
- The most critical stress during the bending of a fully bonded IRP system with any level of internal pressure is the longitudinal tensile stress at the bottom of IRP at the discontinuity edge.

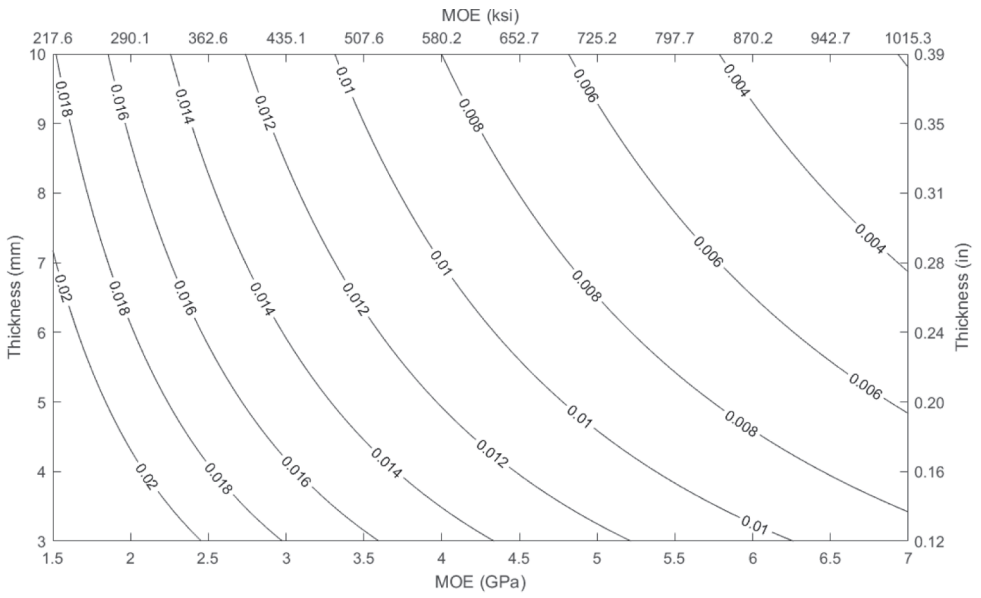

(a)

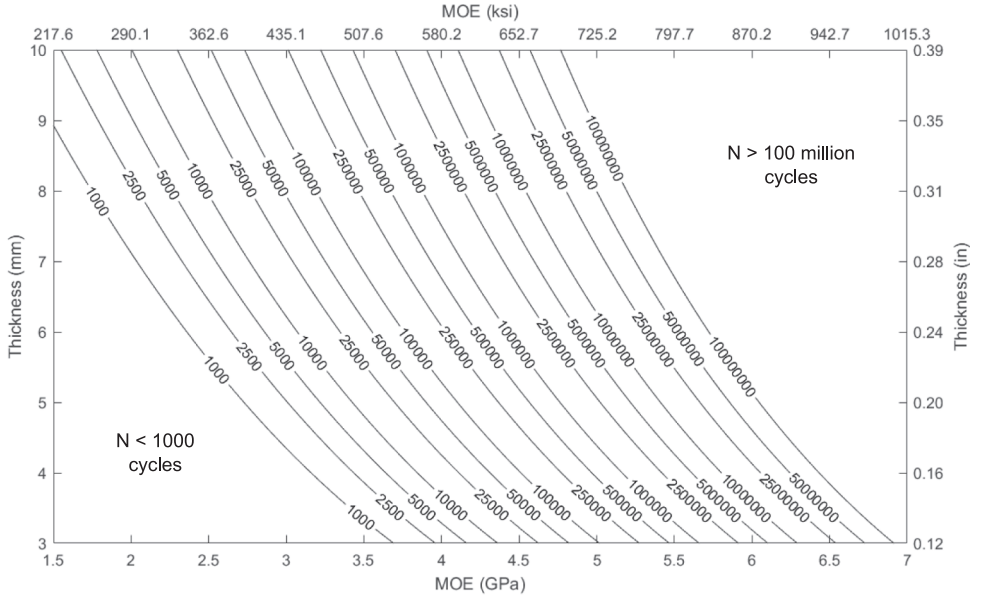

(b)

Fig. 24. (a) Strain and (b) fatigue life responses for varying MOE and thickness subjected to transmitted traffic load of 14.8 kN (3.3 kips) under internal pressure of 413.7 kPa (60.0 psi).

- The increased concentration of longitudinal tensile stresses at the discontinuity edges caused by the rise in internal pressure during bending can significantly shorten the fatigue life of the IRP.
- The level of internal pressure changes the failure behaviour of IRP under bending fatigue. Bulging in the middle of the bottom portion of IRP between the discontinuity edges of the host pipe and bending slightly inward at the top is the failure of the repair system without internal pressure. However, as the internal pressure increases, the bulge at the bottom of IRP becomes more pronounced, while the inward bending at the top disappears.
- The fatigue life of IRP exhibits a slight nonlinear decline with increasing internal pressure under constant transmitted traffic loading. GFRP-1 IRP system having a thickness of 4.115 mm (0.162 in) and being subjected to a transmitted traffic load of 14.8 kN (3.3 kips) can last one million cycles of fatigue loading if the internal pressure remains below 121.3 kPa (17.6 psi).
- The critical tensile stress of IRP systems, whether pressurised or non-pressurized, exhibits a nonlinear decline with increasing repair thickness. The most significant decrease in stress is observed when the repair thickness is increased under the highest internal pressure, whereas the least reduction is noted in the absence of internal pressure.
- The fatigue life of both pressurised and non-pressurized IRP systems increases nonlinearly with respect to repair thickness. To satisfy the design fatigue life criteria at an internal pressure level of zero, 206.8 kPa (30.0 psi), 413.7 kPa (60.0 psi) and 620.5 kPa (90.0 psi), the minimum repair thicknesses required for a transmitted traffic load of 14.8 kN (3.3 kips) are 3.7 mm (0.15 in), 5.3 mm (0.21 in), 7.1 mm (0.28 in) and 8.9 mm (0.35 in), respectively.

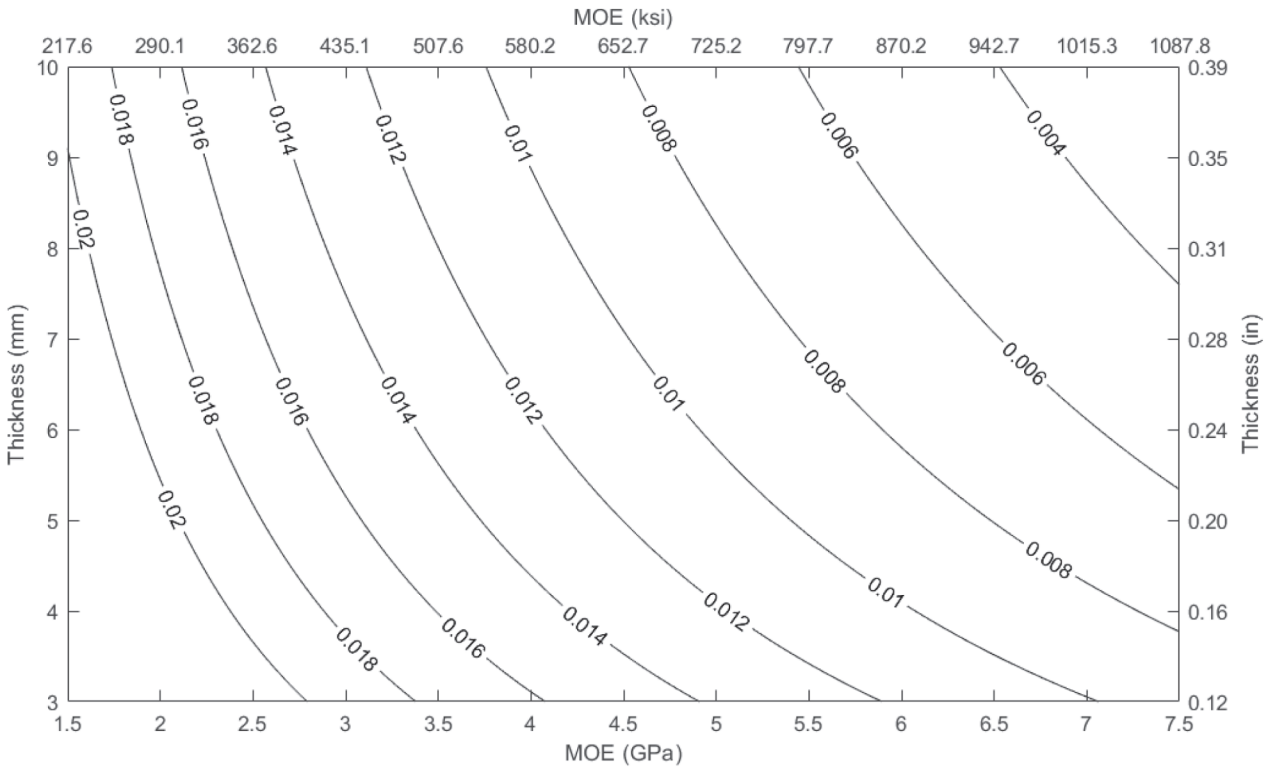

(a)

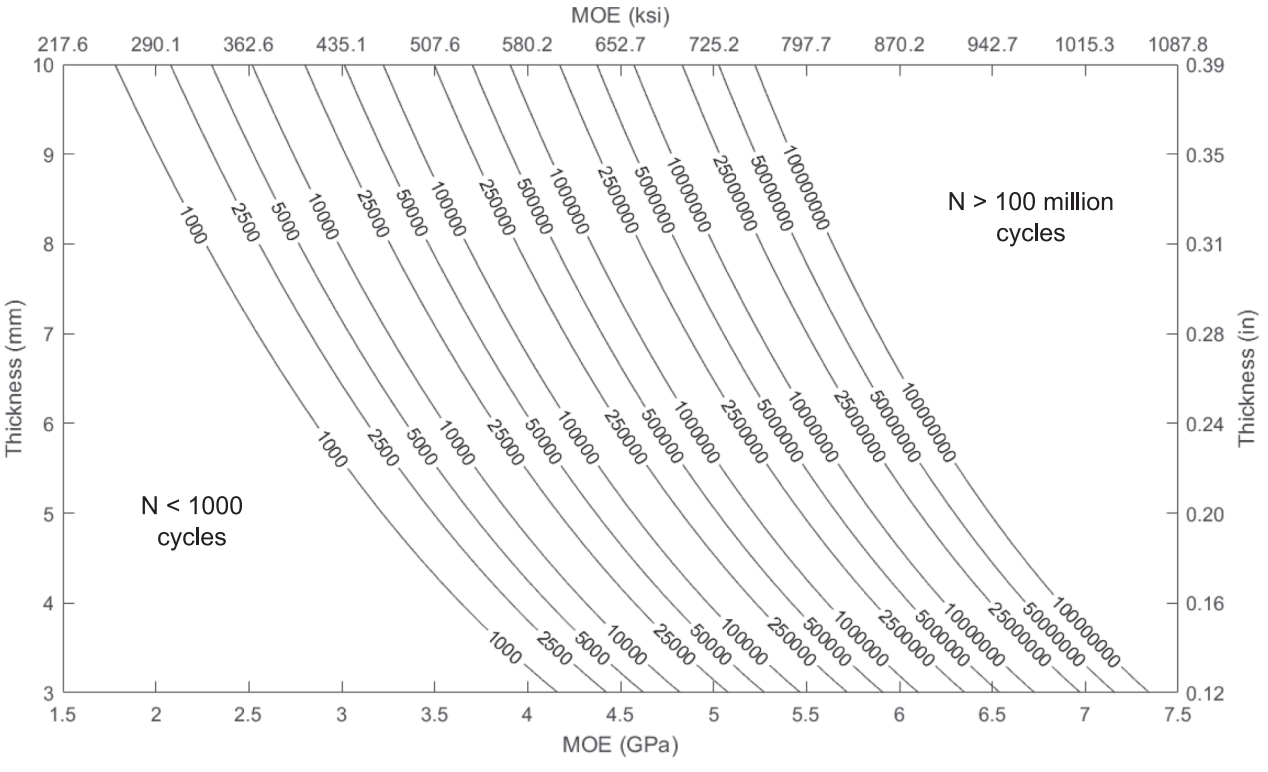

(b)

Fig. 25. (a) Strain and (b) fatigue life responses for varying MOE and thickness subjected to transmitted traffic load of 14.8 kN (3.3 kips) under internal pressure of 620.5 kPa (90.0 psi).

- Polymeric IRP has low resistance under fatigue loading even without internal pressure. To achieve a design fatigue life of one million cycles when exposed to a transmitted traffic load of 14.8 kN (3.3 kips) under internal pressures of zero, 206.8 kPa (30.0 psi), 413.7 kPa (60.0 psi) and 620.5 kPa (90.0 psi), it is necessary for the MOE of IRP with a thickness of 4.115 mm (0.162 in) be at least 3.5 GPa (508 ksi), 4.2 GPa (609 ksi), 4.8 GPa (696 ksi) and 5.3 GPa (769 ksi), respectively.
- Internal repair pipe systems subjected to relatively lower transmitted traffic loads are severely affected by a rise in internal pressure. When tested with a transmitted traffic load of 10.0 kN (2.2 kips), the GFRP-1 IRP system could satisfy the design life requirement under an internal pressure of no more than 389.6 kPa (56.5 psi). Without internal pressure, GFRP-1 IRP systems subjected to transmitted traffic loads of 20.0 kN (4.5 kips) or higher fail to continue functioning up to their intended service life.
- Fatigue lives of IRP systems, regardless of the magnitude of internal pressure, demonstrate a slight nonlinear reduction with an increase in transmitted traffic load. GFRP-1 IRP system with a repair thickness of 4.115 mm (0.162 in) operating at internal pressure levels of zero, 206.8 kPa (30.0 psi), 413.7 kPa (60.0 psi) and 620.5 kPa (90.0 psi), can only achieve the expected fatigue life if the transmitted traffic load level does not exceed 15.8 kN (3.6 kips), 12.4 kN (2.8 kips), 9.7 kN (2.2 kips) and 6.7 kN (1.5 kips), respectively.

The outcomes of extensive parametric investigations have led to the development of simplified mathematical formulas and design charts that aid in predicting the fatigue life of IRP systems. This study will provide valuable insights for engineers and designers, enabling them to make well-informed decisions when selecting the design parameters for IRP systems. By doing so, they can meet the desired design life requirement and achieve more efficient and optimized designs, while reducing cost and time for large-scale experimental testing and evaluation.

CRediT authorship contribution statement

Shanika Kiriella: Writing – review & editing, Writing – original draft, Visualization, Validation, Software, Methodology, Investigation, Formal analysis, Data curation, Conceptualization. **Allan Manalo:** Writing – review & editing, Writing – original draft, Supervision, Resources, Project administration, Methodology, Funding acquisition, Conceptualization. **Cam Minh Tri Tien:** Writing – review & editing, Supervision, Software, Methodology, Conceptualization. **Hamid Ahmadi:** Writing – review & editing, Methodology. **Warna Karunasena:** Writing – review & editing, Supervision, Methodology, Conceptualization. **Patrick G. Dixon:** Writing – review & editing, Validation, Methodology, Conceptualization. **Ahmad Salah:** Software, Methodology, Conceptualization. **Brad P. Wham:** Writing – review & editing, Supervision, Resources, Project administration, Methodology, Funding acquisition, Conceptualization.

Declaration of competing interest

The authors declare that they have no known competing financial interests or personal relationships that could have appeared to influence the work reported in this paper.

Data availability

Data will be made available on request.

Acknowledgement

The information, data, or work presented herein was funded in part by the Advanced Research Projects Agency-Energy (ARPA-E), US Department of Energy, under Award Number DE-AR0001327. The views and opinions of authors expressed herein do not necessarily state or reflect those of the United States Government or any agency thereof.

References

Abd-Elhady, A.A., Sallam, H.-E.-D.-M., Alarifi, I.M., Malik, R.A., EL-Bagory, T.M.A.A., 2020. Investigation of fatigue crack propagation in steel pipeline repaired by glass fiber reinforced polymer. Compos. Struct. 242, 112189.

Akhi, A.H., Dhar, A.S., 2021. Fracture parameters for buried cast iron pipes subjected to internal surface corrosions and cracks. J. Pipeline Sci. Eng. 1 (2), 187–197.

Alabtah, F.G., Mahdi, E., Eliyan, F.F., 2021. The use of fiber reinforced polymeric composites in pipelines: A review. Compos. Struct. 276, 114595.

Allouche, E.N., Alam, S., Simicevic, J., Sterling, R., Condit, W., Matthews, J.C., Selvakumar, A., 2014. A pilot study for retrospective evaluation of cured-in-place pipe (CIPP) rehabilitation of municipal gravity sewers. Tunn. Undergr. Space Technol. 39, 82–93.

Alzabeebee, S., Chapman, D.N., Faramarzi, A., 2018. A comparative study of the response of buried pipes under static and moving loads. Transp. Geotech. 15, 39–46.

Ansys, *Finite Element Analysis (FEA) Software for Structuaral Engineering*. 2021, ANSYS, Inc.

Argyrou, C., O'rourke, T.D., Stewart, H.E., Wham, B.P., 2019. Large-Scale Fault Rupture Tests on Pipelines Reinforced with Cured-in-Place Linings. J. Geotech. Geoenviron. Eng. 145 (3).

ASTM, *ASTM D3479/D3479M-19*, in *Standard Test Method for Tension-Tension Fatigue of Polymer Matrix Composite Materials*. 2019, ASTM International. p. 1-6.

Bokaian, A., 2004. Thermal expansion of pipe-in-pipe systems. Mar. Struct. 17 (6), 475–500.

Brown, M.J.P., Moore, I.D., Fam, A., 2014. Performance of a cured-in-place pressure pipe liner passing through a pipe section without structural integrity. Tunn. Undergr. Space Technol. 42, 87–95.

Budhe, S., Banea, M.D., De Barros, S., 2020. Composite repair system for corroded metallic pipelines: an overview of recent developments and modelling. J. Mar. Sci. Technol. 25, 1308–1323.

Chen, X., Wu, Z., Chen, W., Kang, R., He, X., Miao, Y., 2019. Selection of key indicators for reputation loss in oil and gas pipeline failure event. Eng. Fail. Anal. 99, 69–84.

Chin, W.S., Lee, D.G., 2005. Development of the trenchless rehabilitation process for underground pipes based on RTM. Compos. Struct. 68 (3), 267–283.

Deng, M.L., Bao, C., Hung, A.T.S., Md Noor, N., Lim, K.S., 2022. Effect of defect geometries upon burst capacity of composite repaired pipe. Physics and Chemistry of the Earth, Parts a/b/c 128, 103274.

Dixon, P.G., Tafsirojjaman, T., Klingaman, J., Hubler, M.H., Dashti, S., O'rourke, T.D., Farrag, K.A., Manalo, A., Wham, B.P., 2023. State-of-the-Art Review of Performance Objectives for Legacy Gas Pipelines with Pipe-in-Pipe Rehabilitation Technologies. J. Pipeline Syst. Eng. Pract. 14 (2).

El-Abbasy, M.S., Senouci, A., Zayed, T., Mosleh, F., 2015. A condition assessment model for oil and gas pipelines using integrated simulation and analytic network process. Struct. Infrastruct. Eng. 11 (3), 263–281.

Fajri, A., Prabowo, A.R., Surojo, E., Imaduddin, F., Sohn, J.M., Adiputra, R., 2021. Validation and Verification of Fatigue Assessment using FE Analysis: A Study Case on the Notched Cantilever Beam. Procedia Struct. Integrity 33, 11–18.

Ferdous, W., Manalo, A., Peauril, J., Salih, C., Raghava Reddy, K., Yu, P., Schubel, P., Heyer, T., 2020. Testing and modelling the fatigue behaviour of GFRP composites@ Effect of stress level, stress concentration and frequency. Engineering Science and Technology, an International Journal 23 (5), 1223–1232.

Fu, G., Shannon, B., Azoor, R.M., Ji, J., Deo, R.N., Kodikara, J.K., 2022. Reliability based failure assessment of deteriorated cast iron pipes lined with polymeric liners. Struct. Infrastruct. Eng. 19 (11), 1516–1529.

Fuselli, F., Huber, S.S., Mambretti, S., 2022. Environmental aspects of trenchless pipe rehabilitation methods. Urban Water J. 19, 879–887.

Guo, B., S. Song, J. Chacko, and A. Ghalambor, *Offshore Pipelines*. 1 ed. 2005, Burlington, MA: Elsevier.

Ha, S.K., Lee, H.K., Kang, I.S., 2016. Structural behavior and performance of water pipes rehabilitated with a fast-setting polyurea–urethane lining. Tunn. Undergr. Space Technol. 52, 192–201.

Huang, Z.-Y., Zhang, W., Qian, X., Su, Z., Pham, D.C., Sridhar, N., 2020. Fatigue behaviour and life prediction of filament wound CFRP pipes based on coupon tests. Mar. Struct. 72, 102756.

Huh, Y.H., Lee, J.H., Kim, D., Lee, Y.-S., 2012. Effect of stress ratio on fatigue life of GFRP composites for WT blade. J. Mech. Sci. Technol. 26, 2117–2120.

Jeon, S.-S., O'Rourke, T.D., Neravali, A.N., 2004. Repetitive loading effects on cast iron pipelines with cast-in-place pipe lining system. J. Transp. Eng. 130 (6), 692–705.

Kiriella, S., Manalo, A., Tien, C.M.T., Ahmadi, H., Wham, B.P., Salah, A., Tafsirojjaman, T., Karunasena, W., Dixon, P., O'Rourke, T.D., 2023. Lateral deformation behaviour of structural internal replacement pipe repair systems. Compos. Struct. 319.

Kiriella, S., Manalo, A., Tien, C.M.T., Ahmadi, H., Dixon, P.G., Karunasena, W., Salah, A., Wham, B.P., 2024. Bending fatigue behaviour of internal replacement pipe systems. Compos. Struct. 331, 117910.

Klingaman, J., P.G. Dixon, B.P. Wham, S. Dashti, and M.H. Hubler. *Traffic Loading Effects on Rehabilitated Cast Iron Distribution Pipelines*. in *Pipelines 2022*. 2022. Indianapolis, Indiana.

Kraidi, L., Shah, R., Matipa, W., Borthwick, F., 2019. Analyzing the critical risk factors associated with oil and gas pipeline projects in Iraq. Int. J. Crit. Infrastruct. Prot. 24, 14–22.

Li, B., W.J. Yu, Y.-p. Xie, H. Fang, X. Du, N. Wang, K. Zhai, D. Wang, X. Chen, M. Du, M. Sun, and X. Zhao, *Trenchless rehabilitation of sewage pipelines from the perspective of the whole technology chain: A state-of-the-art review*. Tunnelling and Underground Space Technology, 2023. **134.**

Liu, W., Guo, Q., Qiao, C., Hou, W., 2019. Strain design method of buried pipeline crossing fault. Eng. Fail. Anal. 105, 659–671.

Lu, H., Behbahani, S., Azimi, M., Matthews, J.C., Han, S., Iseley, T., 2020. Trenchless Construction Technologies for Oil and Gas Pipelines: State-of-the-Art Review. Journal of Construction Engineering and Management-Asce 146 (6), 03120001.

Makar, J.M., R. Desnoyers, and S.E. McDonald, *Failure modes and mechanisms in gray cast iron pipe*. 1 ed. 2001, Ottawa, Ontario, Canada: Institute for Research in Construction, National Research Council Canada. 10.

Mattos, H.d.C., J.M.L. Reis, L.M. Paim, M.L.d. Silva, R.L. Junior, and V.A. Perrut, *Failure analysis of corroded pipelines reinforced with composite repair systems.* Engineering Failure Analysis, 2016. **59**: p. 223-236.

Melissianos, V.E., Vamvatsikos, D., Gantes, C.J., 2017. Performance-based assessment of protection measures for buried pipes at strike-slip fault crossings. Soil Dyn. Earthq. Eng. 101, 1–11.

Mellott, S.R., Fatemi, A., 2014. Fatigue behavior and modeling of thermoplastics including temperature and mean stress effects. Polym. Eng. Sci. 54 (3), 725–738.

Nieslony, A., Bohm, M., 2013. Mean stress effect correction using constant stress ratio S-N curves. Int. J. Fatigue 52, 49–56.

Petersen, D.L., Nelson, C.R., Li, G., McGrath, T.J., Kitane, Y., 2010. *Recommended Design Specifications for Live Load Distribution to Buried Structures*. 210, National Research Cooperative Highway Program. Washington, D.C.

Preedawiphat, P., Mahayotsanun, N., Sa-ngoen, K., Noipitak, M., Tuengsook, P., Sucharitpwatskul, S., Dohda, K., 2020. Mechanical Investigations of ASTM A36 Welded Steels with Stainless Steel Cladding. Coatings 10 (9), 844.

Puigoriol-Forcada, J.M., Alsina, A., Salazar-Martín, A.G., Gómez-Gras, G., Pérez, M.A., 2018. Flexural fatigue properties of polycarbonate fused-deposition modelling specimens. Mater. Des. 155, 414–421.

Rohem, N.R.F., Pacheco, L.J., Budhe, S., Banea, M.D., Sampaio, E.M., Barros, S.D., 2016. Development and qualification of a new polymeric matrix laminated composite for pipe repair. Compos. Struct. 152, 737–745.

Shamsuddoha, M., Islam, T., Aravinthan, A.M., Lau, K.-t.A., 2013. Effectiveness of using fibre-reinforced polymer composites for underwater steel pipeline repairs. Compos. Struct. 100, 40–54.

Shirazi, H., Eadie, R.L., Chen, W., 2023. A review on current understanding of pipeline circumferential stress corrosion cracking in near-neutral PH environment. Eng. Fail. Anal. 148.

Shou, K.J., Chen, B.C., 2018. Numerical analysis of the mechanical behaviors of pressurized underground pipelines rehabilitated by cured-in-place-pipe method. Tunn. Undergr. Space Technol. 71, 544–554.

Shou, K.J., Huang, C.C., 2020. Numerical analysis of straight and curved underground pipeline performance after rehabilitation by cured-in-place method. Underground Space 5 (1), 30–42.

Sirimanna, C.S., A.C. Manalo, W. Karunasena, S. Banerjee, and L. McGarva, *13 - Fiber-reinforced polymer (FRP) repair systems for corroded steel pipelines*, in *Rehabilitation of Pipelines Using Fiber-reinforced Polymer (FRP) Composites*, V.M. Karbhari, Editor. 2015, Woodhead Publishing. p. 267-285.

Stewart, H.E., A.N. Netravali, and T.D. O'Rourke, *Performance Testing of Field-Aged Cured-in-Place Liners (CIPL) for Cast Iron Piping* 2015: School of Civil and Environmental Engineering, Cornell University p. 1-128.

Susmel, L., Tovo, R., Lazzarin, P., 2005. The mean stress effect on the high-cycle fatigue strength from a multiaxial fatigue point of view. Int. J. Fatigue 27, 928–943.

Tafsirojjaman, T., Manalo, A., Tien, C.M.T., Wham, B., Salah, A., Kiriella, S., Karunasena, W., Dixons, P., 2022. Analysis of failure modes in pipe-in-pipe repair systems for water and gas pipelines. Eng. Fail. Anal. 140.

Tien, C.M.T., Manalo, A., Dixon, P., Tafsirojjaman, T., Karunasena, W., Flood, W.W., Ahmadi, H., Kiriella, S.H., Salah, A.M., Wham, B.P., 2023. Effects of the legacy pipe ends on the behaviour of pipe-in-pipe repair systems under internal pressure. Eng. Fail. Anal. 144.

Vasseghi, A., Haghshenas, E., Soroushian, A., Rakhshandeh, M., 2021. Failure analysis of a natural gas pipeline subjected to landslide. Eng. Fail. Anal. 119.

Vazouras, P., Karamanos, S.A., Dakoulas, P.C., 2012. Mechanical behavior of buried steel pipes crossing active strike-slip faults. Soil Dyn. Earthq. Eng. 41, 164–180.

Velázquez, J.C., González-Arévalo, N.E., Díaz-Cruz, M., Cervantes-Tobón, A., Herrera-Hernández, H., Hernández-Sánchez, E., 2022. Failure pressure estimation for an aged and corroded oil and gas pipeline: A finite element study. J. Nat. Gas Sci. Eng. 101, 104532.

Wang, R., Wang, F., Xu, J.-G., Zhong, Y.-H., Shikun, L., 2019. Full-scale experimental study of the dynamic performance of buried drainage pipes under polymer grouting trenchless rehabilitation. Ocean Eng. 181, 121–133.

Xu, D., Chen, L., Yu, C., Zhang, S., Zhao, X., Lai, X., 2023. Failure analysis and control of natural gas pipelines under excavation impact based on machine learning scheme. Int. J. Press. Vessel. Pip. 201, 104870.

Yahong, Z., Sheng, H., Baosong, M., Cong, Z., Xuefeng, Y., Zhongsen, T., Han, L., Caiying, D., 2023. Experiment and evaluation model of liner design for renewal of deteriorated reinforced concrete pipes utilizing cured-in-place-pipe technology. Tunn. Undergr. Space Technol. 132.

Zakaria, K.A., Jimit, R.H., Ramli, S.N.R., Aziz, A.A., Bapokutty, O., Ali, M.B., 2016. Study On Fatigue Life And Fracture Behaviour Of Fibreglass Reinforced Composites. Journal of Mechanical Engineering and Sciences 10 (3), 2300–2310.

Zhang, C., Chen, H., Huang, T.-L., 2018. Fatigue damage assessment of wind turbine composite blades using corrected blade element momentum theory. Measurement 129, 102–111.

Zhang, Y., Wong, R.-C.-K., 2023. Effect of corrosion on buried pipe responses under external load: Experimental and numerical study. Tunn. Undergr. Space Technol. 132, 104934.

Zhong, Z., Wang, S., Zhao, M., Du, X.-L., Li, L., 2018. Performance of ductile iron push-on joints rehabilitated with CIPP liner under repetitive and seismic loadings. Soil Dyn. Earthq. Eng. 115 (776–786).